Downloaded from https://www.cambridge.org/core. IP address: 2.34.25.197, on 04 May 2026 at 12:12:30, subject to the Cambridge Core terms of use, available at https://www.cambridge.org/core/terms. https://doi.org/10.1017/jfm.2026.11233

J. Fluid Mech. (2026), *vol.* 1030, A6, doi:10.1017/jfm.2026.11233

JFM PAPERS

Turbulence-informed kinetic theory of inertial-range fibre fragmentation

Andrea Mazzino[1,2]

[1]Department of Civil, Chemical and Environmental Engineering, DICCA, Via Montallegro 1,
Genova 16145, Italy

[2]Istituto Nazionale di Fisica Nucleare, Sezione di Genova, INFN, Via Dodecaneso 33, Genova 16146, Italy

Corresponding author: Andrea Mazzino, andrea.mazzino@unige.it

(Received 11 September 2025; revised 26 January 2026; accepted 26 January 2026)

Slender fibres, including textile-derived microplastics, are abundant in aquatic environments and often extend beyond the Kolmogorov length scale. While breakup at dissipative scales has been characterised by velocity-gradient statistics, no closure existed for inertial-range spans where eddy turnover sets the clock. Here we develop a turbulence-informed kinetic theory of fibre fragmentation bridging turbulence forcing and slender-beam mechanics. First, we derive a load-to-curvature mapping showing that spanwise forcing generates peak bending moments scaling as $\sim U_L L^2$, with U_L the velocity increment across fibre length L. Second, we construct a breakup hazard $h(L)$ from curvature-threshold exceedances over eddy-time blocks, which identifies a turbulence-defined critical span ℓ_c. For $L > \ell_c$, breakup is eddy-time-limited, $h(L) = O(\bar{\varepsilon}^{1/3} L^{-2/3})$ with $\bar{\varepsilon}$ the mean turbulent energy dissipation rate, whereas for $L < \ell_c$, it is a rare-event process with $h(L) \propto L^{5/3+\alpha}$, α denoting the small correction from intermittency. Embedding this hazard in a self-similar binary kernel yields a closed population-balance equation for the fragment distribution $n(L,t)$ with sources and sinks. The framework produces explicit predictions: intermittency-corrected curvature scalings, critical spans set by material and flow parameters, start-up and halving times linked to surf-zone conditions and scaling profiles in the cascade. The steady-state bulk distribution on the subcritical branch, with vertical removal induced by horizontal convergence, follows $n(L) \propto L^{-8/3-\alpha} \simeq L^{-2.7}$, in striking agreement with the mean slope $\simeq -2.68$ observed for environmental microfibres in recent surveys. The reported variability of slopes is naturally explained in our framework by the coexistence of supercritical and subcritical branches together with L-dependent removal-driven sinks.

Key words: homogeneous turbulence, intermittency, ocean processes

© The Author(s), 2026. Published by Cambridge University Press. This is an Open Access article, distributed under the terms of the Creative Commons Attribution licence (https://creativecommons.org/licenses/by/4.0/), which permits unrestricted re-use, distribution and reproduction, provided the original article is properly cited.

Downloaded from https://www.cambridge.org/core. IP address: 2.34.25.197, on 04 May 2026 at 12:12:30, subject to the Cambridge Core terms of use, available at https://www.cambridge.org/core/terms. https://doi.org/10.1017/jfm.2026.11233

1. Introduction

Slender fibres are ubiquitous in environmental and industrial turbulence (Chiarini, Rosti & Mazzino 2024; Marchioli, Rosti & Verhille 2026), from textile microfibres and fishing-line fragments released along coasts to engineered fibrous suspensions (Suaria *et al.* 2020; Liu *et al.* 2022). Oceanic surveys further show that many microplastic fibres observed in surface waters have lengths well above the Kolmogorov length scale η (e.g. Kooi *et al.* 2021), making inertial-range dynamics directly relevant for realistic environmental scenarios. This inertial-range setting contrasts with the extensively studied sub-Kolmogorov limit for non-spherical particles, where the dynamics is governed by local velocity-gradient statistics (Pumir & Wilkinson 2011; Voth & Soldati 2017). Recent reviews have begun to explore fibre-turbulence interactions beyond the dissipative regime. For example, Chiarini *et al.* (2024) provide a comprehensive overview of the dynamics of finite-size fibre-like objects in turbulent flows, focusing on two-way coupling and the resulting turbulence modulation. Similarly, Olivieri, Mazzino & Rosti (2022) report fully resolved simulations of flexible fibres across scales (from sub-Kolmogorov to integral), revealing how elasticity, inertia and concentration affect curvature distributions, alignment and back-reaction on the flow. Complementing these studies, Brizzolara *et al.* (2021) introduced fibre tracking velocimetry, an experimental technique in which rigid fibres of prescribed length are tracked to probe two-point statistics of turbulence, thereby enabling direct access to fluctuations at inertial or dissipative scales. Together, these studies highlight the need to extend small-scale fibre-fracture models toward the inertial range, where fragmentation controls the fate and length spectra of fibrous debris (e.g. microplastics) advected from rivers into the surf zone and beyond (Zhao *et al.* 2025).

Most direct studies of fibre fracture in homogeneous and isotropic turbulence (HIT) address the sub-Kolmogorov limit. In that limit the fibre experiences a locally smooth flow; its dynamics along a Lagrangian path is governed by the instantaneous velocity-gradient tensor, leading to stretching, intermittent buckling, and two dominant failure modes (tensile versus flexural) controlled by an effective flexibility. Within this framework, Allende *et al.* (2018, 2020) combined theory and direct numerical simulation (DNS) to investigate the two dominant fibre-breakup mechanisms (tensile and flexural failure) for small inextensible fibres in turbulence, as well as the resulting breakup statistics and daughter-size distributions. They show that this fragmentation dynamics is governed by the local Lagrangian velocity-gradient statistics and characterise how the evolution of the length distribution unfolds in time. While their results provide the essential ingredients, statistical laws of breakup and daughter fibre sizes, for constructing population-balance models in the sub-Kolmogorov limit, they do not yet present formal expressions for hazard functions and daughter kernels. Moreover, their scope is inherently limited by the length-scale assumption $L \ll \eta$. While highly valuable in this regime, such models do not yet capture eddy-turnover-limited hazards for spans in the inertial range, nor do they account for the impact of intermittency at coarse-grained scales on curvature statistics, or the spanwise-odd loading that arises when finite-length beams are subjected to strain variations along their span. Extending these approaches to the inertial range therefore requires careful adaptation and further development.

A parallel and mature literature treats the fragmentation of compact objects–solid/floc aggregates and droplets-using population-balance equations calibrated on dissipation-scale stresses. For aggregates in HIT, models and simulations specify breakup rates as functions of hydrodynamic stress and report daughter distributions, enabling kinetic descriptions of mass or size distributions (Bäbler *et al.* 2008; Babler *et al.* 2015). Methodologically, the hazard-kernel-population-balance equation architecture is exactly what is needed for fibres as well. Physically, however, compact-body closures rely on

Downloaded from https://www.cambridge.org/core. IP address: 2.34.25.197, on 04 May 2026 at 12:12:30, subject to the Cambridge Core terms of use, available at https://www.cambridge.org/core/terms. https://doi.org/10.1017/jfm.2026.11233

near-η stress criteria and do not include the bending mechanics specific to slender beams under spanwise-odd loads. Moreover, when $L \gg \eta$ the relevant time scale is the eddy-turnover time at scale L, and the statistics entering the hazard are those of coarse-grained dissipation and velocity increments, not single-point viscous stress. Even for droplets, where fully resolved simulations report Poissonian (‘memoryless’) breakup with a Weber-number-controlled rate (Vela-Martín & Avila 2022), this phenomenology does not straightforwardly transfer to slender fibres: their failure is governed by bending-induced curvature exceedances of a material threshold (set by the flexural rigidity EI and flaw statistics), which yields a strongly length- and orientation-dependent hazard and a distinct scaling structure.

Experimental evidence specific to inertial-range fibre fragmentation shows that turbulence–structure coupling can arrest the cascade at a physical small-scale cutoff. In turbulence experiments with deformable elastic objects that break in the inertial range, Brouzet *et al.* (2021) demonstrated an accumulation of fragments just above a cutoff length set by the fluid–structure interaction, rather than by material brittleness alone. This is a key qualitative constraint for any kinetic theory in the inertial range. However, while that study did introduce a statistical population-balance equation for the fragment-length distribution, the breakup probability $p(L)$ is inferred from curvature statistics and the model time scale is not tied to a physical clock; a turbulence-informed closure of the hazard in terms of inertial-range quantities (e.g. coarse-grained dissipation or eddy time) was not provided by the authors.

On the mathematical side, the kinetics of fragmentation is well understood in abstract settings. Self-similar fragmentation kernels lead to freely decaying or steady-state solutions; moments satisfy closed balance laws; and similarity profiles display branch-dependent asymptotics (Ziff & McGrady 1985; Escobedo, Mischler & Rodriguez Ricard 2005). Monographs survey a broad toolkit for coagulation–fragmentation equations (Bertoin 2006; Banasiak, Lamb & Laurençot 2019).

What is missing for inertial-range fibres is a physics-grounded bridge from turbulence and slender-beam mechanics to the kinetic coefficients: (i) a load-to-curvature map that isolates the spanwise-odd forcing at scale L; (ii) a breakup hazard $h(L)$ derived from curvature-threshold exceedances over eddy-time blocks, distinguishing an eddy-time-limited regime for larger spans from a rare-event regime for smaller spans; and (iii) a closure for the daughter-length distribution to complete the kinetic description; in the low-inertia (overdamped) regime considered here, breakup events are effectively binary (Brouzet *et al.* 2021), motivating a minimal self-similar, exchange-symmetric binary daughter kernel.

The present work addresses these gaps by formulating a turbulence-informed kinetic framework for the fragmentation of slender fibres whose spans lie in the inertial range. Filling this gap is not only of theoretical interest but also of direct relevance to marine microplastics. Field surveys consistently report power-law spectra for the length distribution of microplastic fibres, yet the physical origin of these scaling laws remains unresolved (Kooi *et al.* 2021). A physics-grounded kinetic theory of inertial-range fibre fragmentation can therefore provide a mechanistic basis for interpreting the observed distributions, linking turbulence–structure interactions to the fate and scaling properties of fibrous debris in the ocean.

The paper is organised as follows. Section 2 introduces the fibre model, notation and kinematic conventions. Section 3 defines the residual normal velocity and the quasi-static regime. Section 4 develops the load-to-curvature map and the block-peak moments. Section 5 connects turbulent intermittency to curvature statistics via refined similarity, defines intermittency-corrected critical spans, and quantifies their dependence on material

Downloaded from https://www.cambridge.org/core. IP address: 2.34.25.197, on 04 May 2026 at 12:12:30, subject to the Cambridge Core terms of use, available at https://www.cambridge.org/core/terms. https://doi.org/10.1017/jfm.2026.11233

and flow parameters. Section 6 links these statistics to fracture exceedance and derives necessary conditions and moment-based bounds. Section 7 formulates the fragmentation cascade as a continuous kinetics, embedding the hazard and daughter kernel into a population-balance equation with sources and sinks, and develops the self-similar description and typical-size dynamics. Section 8 collects the main scaling laws for the kinematic response, the self-similar transient regime and the stationary bulk. Section 9 connects the theoretical predictions to environmental observations of microfibre size distributions. Finally, § 10 offers conclusions and perspectives.

2. Fibre model

Before starting the analysis, we remark that, as a general rule, symbols are defined upon first use in the text; for ease of reference, however, a complete list is provided in Appendix A (table 1).

We consider slender, elastic Euler–Bernoulli fibres (Timoshenko & Goodier 1970) of span L and (effective) radius a, with high aspect ratio $\equiv L/a \gg 1$. We write E for the Young's modulus, I for the second moment of area (about the neutral axis) and EI for the flexural rigidity, so that the internal-bending torque T along the fibre and the fibre curvature κ are related by $T = EI\,\kappa$. The symbol κ_{frac} denotes the material curvature threshold for brittle failure, a parameter controlled by embrittlement and flaw statistics (Weibull 1951; Peterson 1974; Anderson 2017). The fibres are neutrally buoyant, overdamped and embedded in homogeneous, isotropic turbulence; unless stated otherwise we focus on spans in the inertial range $L \gg \eta$, η being the Kolmogorov scale (Frisch 1995). The centreline is $\boldsymbol{r}(s, t)$, where the arclength coordinate is $s \in [-L/2, L/2]$. The unit tangent and the projector onto its normal plane are

$$\boldsymbol{t}(s, t) = \partial_s \boldsymbol{r}(s, t), \qquad \|\boldsymbol{t}\| = 1, \qquad \boldsymbol{P}(s, t) = \quad - \boldsymbol{t}(s, t)\,\boldsymbol{t}(s, t). \tag{2.1}$$

Midpoint quantities carry a subscript 0: $\boldsymbol{r}_0 \equiv \boldsymbol{r}(0, t)$, $\boldsymbol{t}_0 \equiv \boldsymbol{t}(0, t)$, $\boldsymbol{P}_0 \equiv \quad - \boldsymbol{t}_0\boldsymbol{t}_0$. A fixed unit normal at the midpoint is denoted by $\boldsymbol{n}_0 \perp \boldsymbol{t}_0$.

We repeatedly use the standard decomposition of the fluid velocity gradient at the midpoint (Batchelor 1970; Tennekes & Lumley 1972; Kim & Karrila 1991), where $\boldsymbol{u}$ (and thus $(\nabla \boldsymbol{u})_0$) is understood as the coarse-grained (filtered at scale L) velocity field in the neighbourhood of the fibre (eddy-scale field). In particular, $\boldsymbol{u}(\boldsymbol{r}_0, t)$ defines the rigid-body translation and the antisymmetric part of $(\nabla \boldsymbol{u})_0$ defines the rigid-body rotation of the co-moving/co-rotating frame. Accordingly,

$$(\nabla \boldsymbol{u})_0 = \boldsymbol{S}_0 + \boldsymbol{W}_0, \qquad \boldsymbol{S}_0^{\top} = \boldsymbol{S}_0, \quad \boldsymbol{W}_0^{\top} = -\boldsymbol{W}_0, \quad \boldsymbol{W}_0\boldsymbol{x} = \quad {}_0 \quad \boldsymbol{x}, \tag{2.2}$$

so that $\boldsymbol{S}_0$ is the rate-of-strain tensor and $\boldsymbol{W}_0$ generates the rigid-body rotation associated with the vorticity $\quad {}_0$.

For a very slender filament ($L \gg a$), the Stokes traction per unit length admits the resistive-force form (Gray & Hancock 1955; Batchelor 1970; Cox 1970; Lighthill 1976; Kim & Karrila 1991):

$$\boldsymbol{f}(s, t) = -\Big[\,\xi_{\perp}\,(\quad - \boldsymbol{t}\boldsymbol{t}) + \xi_{\parallel}\,\boldsymbol{t}\boldsymbol{t}\,\Big]\ \big(\boldsymbol{u}(\boldsymbol{r}(s), t) - \dot{\boldsymbol{r}}(s, t)\quad . \tag{2.3}$$

The leading logarithmic asymptotics gives

$$\xi_{\perp} \simeq \frac{4\pi\mu}{\ln \quad + \delta_{\perp}}, \qquad \xi_{\parallel} \simeq \frac{2\pi\mu}{\ln \quad + \delta_{\parallel}}, \qquad \quad \equiv L/a \gg 1, \tag{2.4}$$

with $\delta_{\perp,\parallel} = O(1)$ and $\xi_\perp/\xi_\parallel \to 2$ as $\quad \to \infty$ (Batchelor 1970; Cox 1970; Kim & Karrila 1991), and where μ is the dynamic viscosity of the fluid.

Since bending is driven by the normal component of the hydrodynamic load, we define the signed normal load entering the Euler–Bernoulli equation for the fibre as

$$q(s,t) \equiv \boldsymbol{n}_0\ \boldsymbol{f}(s,t) \tag{2.5}$$

and compute, using (2.3),

$$\begin{aligned} q(s,t) \equiv \boldsymbol{n}_0\ \boldsymbol{f}(s,t) &= -\,\xi_\perp\, \boldsymbol{n}_0\ (\quad - \boldsymbol{tt})\bigl(\boldsymbol{u} - \dot{\boldsymbol{r}} \quad - \xi_\parallel\, \boldsymbol{n}_0\ \bigl(\boldsymbol{tt}(\boldsymbol{u} - \dot{\boldsymbol{r}}) \\ &= -\,\xi_\perp\Bigl[\boldsymbol{n}_0\ (\boldsymbol{u} - \dot{\boldsymbol{r}}) - (\boldsymbol{n}_0\ \boldsymbol{t})\,\boldsymbol{t}\ (\boldsymbol{u} - \dot{\boldsymbol{r}})\Bigr] - \xi_\parallel(\boldsymbol{n}_0\ \boldsymbol{t})\,\boldsymbol{t}\ (\boldsymbol{u} - \dot{\boldsymbol{r}}). \end{aligned} \tag{2.6}$$

Near the midpoint one has $\boldsymbol{t}(s) = \boldsymbol{t}_0 + O(s)$ and $\boldsymbol{n}_0\ \boldsymbol{t}_0 = 0$, hence $\boldsymbol{n}_0\ \boldsymbol{t} = O(s)$. In the co-moving frame we set $\dot{\boldsymbol{r}}_0 = \boldsymbol{u}(\boldsymbol{r}_0, t)$; therefore, for $\boldsymbol{\phi}(s) \equiv \boldsymbol{u}(\boldsymbol{r}(s), t) - \dot{\boldsymbol{r}}(s,t)$ one has $\boldsymbol{\phi}(0) = \quad$ and, by Taylor expansion of the coarse-grained (eddy-scale) velocity field at scale L used throughout (hence smooth in a neighbourhood of the fibre), $\boldsymbol{\phi}(s) = O(s)$. Consequently $\boldsymbol{t}\ \boldsymbol{\phi}(s) = O(s)$ and the parallel contributions (i.e. the explicit term $-\xi_\parallel\, \boldsymbol{n}_0$ $[\boldsymbol{tt}\,\boldsymbol{\phi}]$ and the leakage $+\xi_\perp\ (\boldsymbol{n}_0\ \boldsymbol{t})\,\boldsymbol{t}\ \boldsymbol{\phi}$ inside the $\xi_\perp$-bracket) are $O(s) \quad O(s) = O(s^2)$, hence negligible at first order. This leaves

$$q(s,t)\ \simeq\ -\,\xi_\perp\, \boldsymbol{n}_0\ \bigl(\boldsymbol{u}(\boldsymbol{r}(s), t) - \dot{\boldsymbol{r}}(s,t) \quad , \tag{2.7}$$

the symbol $\simeq$ indicating the neglect of $O(s^2)$ terms.

A spatially uniform translation and the rigid rotation induced by $\quad_0$ do not bend the fibre; they merely advect/rotate it as a whole. We thus remove those components by working in a co-moving, co-rotating frame at $s = 0$, as shown in the next section.

3. Residual normal velocity

The load-to-curvature reduction adopted here (co-moving/co-rotating frame) assumes that the fibre adjusts quasi-statically to the local turbulent straining. In practice, this requires the visco-elasto-hydrodynamic relaxation of bending to be much faster than the evolution of the eddy at the same span L. When this separation holds, the instantaneous load profile and the ensuing scaling laws are controlled kinematically. Accordingly, let $\tau_L \sim \bar{\varepsilon}^{-1/3} L^{2/3}$ be the eddy turnover time at scale L (Frisch 1995). In the overdamped regime, bending relaxes diffusively under viscous drag with (Powers 2010; Rosti *et al.* 2018)

$$\tau_{visc} \sim \frac{\xi_\perp\, L^4}{EI}. \tag{3.1}$$

The quasi-static requirement $\tau_{visc} \ll \tau_L$ reads

$$\frac{\xi_\perp}{EI}\, L^4 \ll \bar{\varepsilon}^{-1/3}\, L^{2/3} \qquad \Longleftrightarrow \qquad L \ll L_{QS} \equiv \left(\frac{EI\ \bar{\varepsilon}^{-1/3}}{\xi_\perp}\right)^{3/10}, \tag{3.2}$$

or, in non-dimensional form, $L/\mathcal{L} \ll (EI/(\xi_\perp\, u_{rms}\, \mathcal{L}))^{3/10}$ where u_{rms} is the root-mean-square velocity at the integral scale $\mathcal{L}$.

Note that (3.2) is a scaling criterion up to $O(1)$ constants set by the first-mode shape and the eddy-time prefactor. Also note that, in a full inextensible-filament formulation, an additional axial-tension contribution may enter the force balance. In the present work, we restrict to the quasi-static window $L \ll L_{QS}$, where the leading-order response is bending-dominated and tension yields only higher-order corrections. For $L \quad L_{QS}$, tension may

Downloaded from https://www.cambridge.org/core. IP address: 2.34.25.197, on 04 May 2026 at 12:12:30, subject to the Cambridge Core terms of use, available at https://www.cambridge.org/core/terms. https://doi.org/10.1017/jfm.2026.11233

Downloaded from https://www.cambridge.org/core. IP address: 2.34.25.197, on 04 May 2026 at 12:12:30, subject to the Cambridge Core terms of use, available at https://www.cambridge.org/core/terms. https://doi.org/10.1017/jfm.2026.11233

become comparable and a coupled tension-bending treatment would be required, which we, however, do not pursue here.

We now remove rigid-body translation and rotation. Introducing $\delta \boldsymbol{r}(s) = \boldsymbol{r}(s, t) - \boldsymbol{r}_0$, a Taylor expansion about $\boldsymbol{r}_0$ yields

$$\boldsymbol{u}(\boldsymbol{r}(s), t) = \boldsymbol{u}(\boldsymbol{r}_0, t) + (\ \boldsymbol{S}_0 + \boldsymbol{W}_0\ )\, \delta \boldsymbol{r}(s) + O(\|\delta \boldsymbol{r}\|^2), \tag{3.3}$$

while arclength geometry gives

$$\delta \boldsymbol{r}(s) = \int_0^s \boldsymbol{t}(\sigma, t)\, \mathrm{d}\sigma = s\, \boldsymbol{t}_0 + O(s^2). \tag{3.4}$$

In the quasi-static limit, the midpoint may translate with the (solid) velocity $\boldsymbol{u}_s(\boldsymbol{r}_0, t) \equiv \dot{\boldsymbol{r}}_0$, and the spanwise relative velocity due to rigid rotation is $\boldsymbol{W}_0\, \delta \boldsymbol{r}$:

$$\dot{\boldsymbol{r}}_0 = \boldsymbol{u}_s(\boldsymbol{r}_0, t), \qquad \dot{\boldsymbol{r}}(s, t) - \dot{\boldsymbol{r}}_0 \approx \boldsymbol{W}_0\, \delta \boldsymbol{r}(s). \tag{3.5}$$

We define the midpoint slip velocity as $\boldsymbol{u}_{slip}(t) \equiv \boldsymbol{u}(\boldsymbol{r}_0, t) - \boldsymbol{u}_s(\boldsymbol{r}_0, t)$.

The normal residual velocity is defined by removing translation and rigid rotation and projecting onto the midpoint normal plane:

$$\boldsymbol{U}_\perp(s, t) \ \equiv\ \boldsymbol{P}_0\big(\boldsymbol{u}(\boldsymbol{r}(s), t) - \boldsymbol{u}_s(\boldsymbol{r}_0, t) - \boldsymbol{W}_0\, \delta \boldsymbol{r}(s)\ \ . \tag{3.6}$$

If $\boldsymbol{u}_{slip} \neq\ \ $, then (3.3)–(3.6) yield an additional s-independent contribution $\boldsymbol{P}_0 \boldsymbol{u}_{slip}(t)$ in $\boldsymbol{U}_\perp$. Since this contribution is spanwise-even, it does not affect the leading-order spanwise-odd forcing extracted as follows; accordingly, we focus on the odd component and drop the slip term.

Combining (3.3)–(3.6) with (3.4) gives the leading spanwise structure

$$\boldsymbol{U}_\perp(s, t) = s\, \boldsymbol{P}_0 \boldsymbol{S}_0 \boldsymbol{t}_0\ +\ O(s^2), \tag{3.7}$$

which is linear and odd in s. Equivalently, the spanwise-odd part of the relative velocity itself reads

$$\boldsymbol{u}(\boldsymbol{r}(s), t) - \dot{\boldsymbol{r}}(s, t) = s\, \boldsymbol{S}_0 \boldsymbol{t}_0\ +\ O(s^2). \tag{3.8}$$

Starting from the definition of the signed normal load in (2.5) and using $\boldsymbol{n}_0\ \ \boldsymbol{t}_0 = 0$ with $\boldsymbol{t}(s) = \boldsymbol{t}_0 + O(s)$ (so that $\boldsymbol{n}_0\ \ \boldsymbol{P}(s) = \boldsymbol{n}_0 + O(s)$),

$$\begin{aligned} q(s, t) &= -\,\xi_\perp\, \boldsymbol{n}_0\ \ \ \boldsymbol{P}(s)\big(\boldsymbol{u}(\boldsymbol{r}(s), t) - \dot{\boldsymbol{r}}(s, t) \\ &= -\,\xi_\perp\, \boldsymbol{n}_0\ \ \ \big(\,[\boldsymbol{P}_0 + O(s)]\,\big[s\, \boldsymbol{S}_0\, \boldsymbol{t}_0 + O(s^2)\big] \\ &= -\,\xi_\perp\, \boldsymbol{n}_0\ \ \ \big(\boldsymbol{P}_0\, \boldsymbol{S}_0\, \boldsymbol{t}_0\ \ s\ +\ O(s^2), \end{aligned} \tag{3.9}$$

where the mixed term $O(s)\ \ \ \ O(s)$ is $O(s^2)$ and is thus negligible at first order.

For compactness in what follows, we define the operational amplitude and the orientation factor as

$$U_L(t) \equiv L\, \|\boldsymbol{P}_0\, \boldsymbol{S}_0\, \boldsymbol{t}_0\|, \qquad \cos\ \ \ (t) \equiv -\,\frac{\boldsymbol{n}_0\ \ \ (\boldsymbol{P}_0\, \boldsymbol{S}_0\, \boldsymbol{t}_0)}{\|\boldsymbol{P}_0\, \boldsymbol{S}_0\, \boldsymbol{t}_0\|}, \tag{3.10}$$

so that the signed load profile reads

$$q(s, t) = \xi_\perp\, U_L(t)\, \frac{\cos\ \ \ (t)}{L}\, s\ +\ O(s^2), \tag{3.11}$$

which is odd in s and produces zero net force on the symmetric span. For scaling purposes, $|\cos\ \ \ | = O(1)$.

Downloaded from https://www.cambridge.org/core. IP address: 2.34.25.197, on 04 May 2026 at 12:12:30, subject to the Cambridge Core terms of use, available at https://www.cambridge.org/core/terms. https://doi.org/10.1017/jfm.2026.11233

4. Load-to-curvature map and block-peak moments

To compute the leading-order internal-bending moment over the whole span, we replace the instantaneous load by its leading-order (LO) odd component q_{LO} about the midpoint (the linear term) and extend it across $[-L/2, L/2]$:

$$q_{LO}(s,t) \equiv q_0(t)\,\frac{s}{L}, \qquad q_0(t) = \xi_\perp\, U_L(t)\cos\quad(t). \tag{4.1}$$

The extension to the whole span is justified because, over eddy-turnover-time intervals at the fibre scale, the rate-of-strain of the coarse-grained velocity field is nearly uniform along the span; in addition, the beam filters turbulence across the span: motions at scales much larger than the fibre length produce near-uniform sweeping, sub-span fluctuations are attenuated, and the fibre-scale forcing dominates.

With free ends, anchoring the internal-bending torque integral at the tip gives, for $0 \leq s \leq L/2$,

$$T(s,t) = \int_s^{L/2} (\zeta - s)\, q_{LO}(\zeta,t)\,\mathrm{d}\zeta = \frac{q_0(t)}{24L}\left(L^2(L-3s)+4s^3\right), \tag{4.2}$$

so that $T(L/2,t)=0$ and the peak occurs at midspan:

$$T_{max}(t) = T(0,t) = \frac{q_0(t)\,L^2}{24} \;\propto\; \xi_\perp\, U_L(t)\, L^2. \tag{4.3}$$

Consistent with (3.10)–(4.3), the fibre acts as a spanwise low-pass filter: κ_ℓ is the curvature contributed by any sub-span scale $\ell \leq L$ scales as

$$\kappa_\ell \sim \frac{\xi_\perp}{EI}\, U_\ell\, \ell^2, \tag{4.4}$$

where U_ℓ denotes the transverse velocity increment across separation ℓ (same definition as U_L with $L \to \ell$). Using inertial-range scaling $U_\ell \sim (\bar{\varepsilon}\,\ell)^{1/3}$, one obtains $\kappa_\ell \propto \ell^{7/3}$. Hence, among all $\ell \leq L$, the largest coherent scale $\ell \simeq L$ dominates, and the relative contribution of a sub-span scale satisfies

$$\frac{\kappa_\ell}{\kappa_L} \sim \frac{U_\ell}{U_L}\left(\frac{\ell}{L}\right)^2 \sim \left(\frac{\ell}{L}\right)^{7/3} \ll 1, \tag{4.5}$$

up to the $O(1)$ orientation factor $|\cos\quad|$ already appearing in (3.10) and (3.11).

To connect the instantaneous load profile to statistically robust peak curvatures, we sample the time series in non-overlapping eddy-time blocks of duration

$$\Delta T = c\,\tau_L, \qquad \tau_L \sim \bar{\varepsilon}^{-1/3} L^{2/3}, \quad c = O(1). \tag{4.6}$$

Within each block $b = [t_b, t_b + \Delta T)$, where t_b denotes the start time of the time block b, the large-scale strain is slowly varying at scale L while rare curvature spikes are captured. Denoting the block-peak curvature as

$$\kappa_{blk}^{(b)} = \max_{t\in b} \frac{T_{max}(t)}{EI} \equiv \frac{T_{max}^{(b)}}{EI}, \tag{4.7}$$

at block level ($\Delta T \sim \tau_L$) we obtain

$$\kappa_{blk}^{(b)} \sim \frac{T_{max}^{(b)}}{EI} \sim \frac{\xi_\perp}{EI}\, U_L^{(b)}\, L^2, \tag{4.8}$$

where (4.3) has been used and

$$U_L^{(b)} \equiv \max_{t\in b}\, U_L(t). \tag{4.9}$$

Downloaded from https://www.cambridge.org/core. IP address: 2.34.25.197, on 04 May 2026 at 12:12:30, subject to the Cambridge Core terms of use, available at https://www.cambridge.org/core/terms. https://doi.org/10.1017/jfm.2026.11233

Hence the pth curvature moment reads

$$M_p(L) \equiv \left\langle \left(\kappa_{blk}^{(b)}\right)^p \right\rangle_b \sim \left(\frac{\xi_\perp}{EI}\right)^p L^{2p} \left\langle (U_L^{(b)})^p \right\rangle_b, \tag{4.10}$$

where block averages at fixed L (or ensemble averages over independent realisations at fixed L) are indicated by $\langle\ \rangle_b$.

We adopt the block/ensemble mean as the typical block-peak curvature:

$$\kappa^\star(L) \equiv M_1(L) = \langle \kappa_{blk}^{(b)} \rangle_b, \tag{4.11}$$

so that

$$\kappa^\star(L) \sim \frac{\xi_\perp}{EI} \langle U_L^{(b)} \rangle_b \, L^2. \tag{4.12}$$

For later use we define the pth moment normalised by the third moment,

$$\widehat{M}_p^{(3)}(L) \equiv \frac{M_p(L)}{M_3(L)^{p/3}} = \frac{\left\langle \left(\kappa_{blk}^{(b)}\right)^p \right\rangle_b}{\left(\left\langle \left(\kappa_{blk}^{(b)}\right)^3 \right\rangle_b\right)^{p/3}}, \qquad p > 0. \tag{4.13}$$

5. Connecting turbulent intermittency to fibre curvature statistics via refined similarity

This section connects turbulent intermittency to fibre curvature statistics and defines the critical spans that separate frequent from rare breakage.

Let ε_L be the coarse-grained dissipation at scale L (spatial average near the fibre), and $\mathcal{L}$ the integral scale. Define the moment-scaling function $\tau(q)$ (Frisch 1995) by

$$\left\langle \left(\frac{\varepsilon_L}{\bar{\varepsilon}}\right)^q \right\rangle \sim \left(\frac{L}{\mathcal{L}}\right)^{\tau(q)}, \qquad L \lesssim \min\{\mathcal{L},\ L_{QS}\}. \tag{5.1}$$

Refined similarity (Kolmogorov 1962) yields, for the pth moment of the transverse velocity increment across separation L, the following relationships valid up to $O(1)$ prefactors:

$$S_p(L) \equiv \langle U_L^p(t) \rangle \sim \left\langle \left(U_L^{(b)}\right)^p \right\rangle_b \sim L^{p/3} \langle \varepsilon_L^{p/3} \rangle. \tag{5.2}$$

Comparing with $S_p(L) \sim L^{\zeta_p}$ yields

$$\tau(q) = \zeta_{3q} - q. \tag{5.3}$$

In particular, for $q = 1/3$,

$$\langle \varepsilon_L^{1/3} \rangle = \bar{\varepsilon}^{1/3} \left(\frac{L}{\mathcal{L}}\right)^\alpha, \qquad \alpha \equiv \tau\!\left(\frac{1}{3}\right) = \zeta_1 - \frac{1}{3}. \tag{5.4}$$

Since $x \mapsto x^{1/3}$ is concave and $\langle \varepsilon_L \rangle = \bar{\varepsilon}$ (stationarity), Jensen's inequality implies $\langle \varepsilon_L^{1/3} \rangle \leq \bar{\varepsilon}^{1/3}$; in (5.4) this corresponds to $\alpha \geq 0$, typically small and positive.

Exploiting (5.2), (4.10) can be recast as

$$M_p(L) \sim \left(\frac{\xi_\perp}{EI}\right)^p L^{2p} L^{p/3} \langle \varepsilon_L^{p/3} \rangle, \tag{5.5}$$

and, using (5.1),

$$M_p(L) \sim \left(\frac{\xi_\perp}{EI}\right)^p \bar{\varepsilon}^{\,p/3} \mathcal{L}^{-\tau(p/3)} L^{\frac{7}{3}p + \tau(p/3)}, \qquad p > 0, \tag{5.6}$$

Downloaded from https://www.cambridge.org/core. IP address: 2.34.25.197, on 04 May 2026 at 12:12:30, subject to the Cambridge Core terms of use, available at https://www.cambridge.org/core/terms. https://doi.org/10.1017/jfm.2026.11233

i.e. the intermittency-corrected scaling of the pth raw moment.

To isolate a pure scaling law where only intermittency is involved, it is convenient to resort to the pth normalised moments (4.13). Using (5.6), the following expression is obtained:

$$\widehat{M}_p^{(3)}(L) \equiv \frac{M_p(L)}{M_3(L)^{\,p/3}} \sim \left(\frac{L}{\mathcal{L}}\right)^{\tau(p/3)}, \qquad p > 0. \tag{5.7}$$

Hence, intermittency is encoded in the L-dependence of the normalised curvature moments: the log–log slope of $\widehat{M}_p^{(3)}(L)$ versus L is exactly $\tau(p/3)$. Moreover, $\widehat{M}_3^{(3)}(L) = 1$ identically, and in the Kolmogorov's 1941 theory (K41) limit ($\tau \equiv 0$) all $\widehat{M}_p^{(3)}(L)$ are L-independent. In a mean-field setting (neglecting intermittency), one replaces $\langle \varepsilon_L^{1/3} \rangle$ with $\bar{\varepsilon}^{1/3}$. Using (4.11) and (5.5) (for $p = 1$), this yields a mean-field estimate of the typical peak-type curvature (i.e. the block-averaged maximum curvature along the span),

$$\kappa^\star_{MF}(L) \equiv \langle \kappa^{(b)}_{blk} \rangle_b \simeq \frac{\xi_\perp}{EI}\, \bar{\varepsilon}^{1/3}\, L^{7/3}, \tag{5.8}$$

from which the definition of the mean-field critical span ℓ_c by $\kappa^\star_{MF}(\ell_c) = \kappa_{frac}$ naturally emerges. Namely,

$$\ell_c = \left(\frac{\kappa_{frac}\, EI}{\xi_\perp\, \bar{\varepsilon}^{1/3}}\right)^{3/7}. \tag{5.9}$$

We remark that the quasi-static bound in (3.2) defines the scale $L_{QS} = (EI\, \bar{\varepsilon}^{-1/3}/\xi_\perp)^{3/10}$ up to $O(1)$ constants (first-mode shape and eddy-time prefactor); it is a scaling criterion, not a hard numerical cutoff. By contrast, the critical size ℓ_c from (5.9) is a material threshold set by the block-peak curvature balance and, for consistency with the quasi-static assumption, should fall within the quasi-static window (i.e. $\ell_c \lesssim L_{QS}$ up to those $O(1)$ constants).

The scaling $\kappa^\star_{MF}(L) \propto L^{7/3}$ in (5.8) refers to a peak-type curvature (the block-peak over an eddy-time interval at scale L) obtained from the instantaneous Euler–Bernoulli mapping with $U_L \sim (\bar{\varepsilon} L)^{1/3}$. This is fully consistent with Olivieri *et al.* (2022), who analyse the spanwise maximum curvature at each instant (then averaged over time/realisations) and, in the linear-bending regime, obtain the same $L^{7/3}$ exponent. By contrast, Brouzet *et al.* (2021) analyse the time/ensemble-averaged curvature profile and report that its maximum scales as L^3 for short fibres ($L < 1$ in elastic-length units), and that this maximum approaches an order-one constant for $L \quad 1$. This is a different observable (the maximum of the averaged profile) from our peak-type measure (the mean, over eddy-time blocks, of the instantaneous spanwise maxima), so distinct exponents are expected and no contradiction arises.

Including now intermittency, the order-1 critical span $\ell_c^{(1)}$ (defined by $\kappa^\star(\ell_c^{(1)}) = \kappa_{frac}$ with $\kappa^\star(L) \propto L^{7/3+\alpha} \mathcal{L}^{-\alpha}$, $\alpha = \tau(1/3)$) relates to ℓ_c via

$$\ell_c^{(1)} = \ell_c \left(\frac{\mathcal{L}}{\ell_c}\right)^{\frac{\alpha}{7/3+\alpha}} \simeq \ell_c \left[1 + \frac{3}{7}\alpha \ln\!\left(\frac{\mathcal{L}}{\ell_c}\right)\right] \quad (\alpha \ll 1). \tag{5.10}$$

It is convenient to introduce the dimensionless loading parameters

$$y_1(L) \equiv \frac{\kappa^\star(L)}{\kappa_{frac}} = \left(\frac{L}{\ell_c^{(1)}}\right)^{7/3+\alpha}, \qquad \theta(L) \equiv \frac{\kappa_{frac}}{\kappa^\star(L)} = \frac{1}{y_1(L)}. \tag{5.11}$$

Downloaded from https://www.cambridge.org/core. IP address: 2.34.25.197, on 04 May 2026 at 12:12:30, subject to the Cambridge Core terms of use, available at https://www.cambridge.org/core/terms. https://doi.org/10.1017/jfm.2026.11233

Two regimes follow: for $L < \ell_c^{(1)}$ (i.e. $y_1 < 1$, $\theta > 1$) exceedances are rare (subcritical); for $L > \ell_c^{(1)}$ (i.e. $y_1 > 1$, $\theta < 1$) exceedances are frequent (supercritical). In the non-intermittent limit ($\alpha = 0$) one simply has $y_1(L) = (L/\ell_c)^{7/3}$.

Given the pth raw moment of the block-peak curvature $M_p(L) = \left\langle (\kappa_{blk}^{(b)})^p \right\rangle_b$ and its intermittency-corrected scaling in (5.6), the moment-based critical span $\ell_c^{(p)}$ is defined as the scale at which the pth moment reaches the material threshold to the pth power:

$$M_p\big(\ell_c^{(p)} \ = \kappa_{frac}^{p}, \qquad p > 0. \tag{5.12}$$

Using (5.6) gives

$$\ell_c^{(p)} = \left(\frac{\kappa_{frac}\, EI}{\xi_\perp\, \bar{\varepsilon}^{1/3}} \right)^{\frac{p}{\frac{7}{3}p + \tau(p/3)}} \mathcal{L}^{\frac{\tau(p/3)}{\frac{7}{3}p+\tau(p/3)}}, \qquad p > 0. \tag{5.13}$$

In the K41 limit, $\tau(p/3) = 0$ and $\ell_c^{(p)}$ becomes independent of p, namely $\ell_c^{(p)} = \ell_c = (\kappa_{frac}\, EI/(\xi_\perp\, \bar{\varepsilon}^{1/3}))^{3/7}$. Since $\tau(q) = \zeta_{3q} - q$ is concave with $\tau(1) = 0$, one has $\tau(p/3) > 0$ for $p < 3$, $\tau(p/3) = 0$ for $p = 3$, and $\tau(p/3) < 0$ for $p > 3$. Consequently, $\ell_c^{(p)}$ increases relative to K41 for $p < 3$, is unchanged at $p = 3$, and can decrease for $p > 3$, with the deviation growing with $|\tau(p/3)|$.

We conclude this section with a remark to clarify the scope and robustness of our use of $\tau(q)$. Here $\tau(q)$ is employed solely as a compact descriptor for the L-dependence of coarse-grained dissipation moments in the normalised-moment diagnostic (5.7); we neither adopt nor adjudicate between specific mechanisms (e.g. finite-Reynolds-number effects versus ‘intermittency’) behind departures from pure K41 scaling. All fragmentation predictions developed below-load-to-curvature mapping, eddy-time-limited branch, critical span and bulk slopes remain valid with $\tau \equiv 0$, and small departures (when present) only tilt this diagnostic without altering the regime structure. For completeness, recent discussions of finite-Reynolds number effects on small-scale departures from K41 are available in the literature (e.g. Tang *et al.* 2017, 2020, 2023), but our use of $\tau(\ )$ here is purely notational and does not affect the fragmentation results.

6. Fracture exceedance: necessary condition and moment bounds

We link the fibre-level kinematics to exceedance probabilities for curvature-threshold fracture. First, a necessary condition expresses fracture as an increment-threshold event. Then, without assuming a specific tail shape, we derive non-parametric upper and lower bounds directly from curvature moments, consistent with refined similarity.

6.1. *Necessary condition via an increment threshold*

From the load-to-curvature map, the block peak obeys (up to $O(1)$ factors)

$$\kappa_{blk}^{(b)} \simeq \frac{\xi_\perp}{EI} L^2\, U_L^{(b)}\, C^{(b)}, \qquad C^{(b)} \equiv |\cos\ \ ^{(b)}| \in [0, 1], \tag{6.1}$$

where $U_L^{(b)} \equiv \max_{t \in b} U_L(t)$ is the operational shear amplitude at scale L, and $C^{(b)}$ is the orientation factor ((3.10)).

The dynamic velocity threshold is defined as

$$u_{thr}(L) \equiv \frac{EI}{\xi_\perp} \frac{\kappa_{frac}}{L^2} \propto L^{-2}, \tag{6.2}$$

Downloaded from https://www.cambridge.org/core. IP address: 2.34.25.197, on 04 May 2026 at 12:12:30, subject to the Cambridge Core terms of use, available at https://www.cambridge.org/core/terms. https://doi.org/10.1017/jfm.2026.11233

which shows that shorter spans are harder to break. Then the block fracture probability is

$$p_{block}(L) \;=\; {}_{C}\left[\mathbb{P}\left(U_L^{(b)} > \frac{u_{thr}(L)}{C}\,\middle|\, C\right)\right], \tag{6.3}$$

where $\mathbb{P}(\ )$ denotes probability and ${}_{C}[\ ]$ denotes expectation with respect to the distribution of the random orientation factor $C \in [0, 1]$ (here $C \equiv |\cos\ ^{(b)}|$).

For every fixed $c \in (0, 1]$, the events satisfy

$$\left\{\, U_L^{(b)} > \frac{u_{thr}(L)}{c} \,\right\} \subseteq \left\{\, U_L^{(b)} > u_{thr}(L) \,\right\}, \tag{6.4}$$

hence, averaging with respect to the law of C and using the law of total probability,

$$p_{block}(L) \;\leq\; \mathbb{P}\Big(U_L^{(b)} > u_{thr}(L)\Big)\,. \tag{6.5}$$

Deterministically, fracture requires

$$U_L^{(b)}\, C^{(b)} \;>\; u_{thr}(L), \qquad C^{(b)} \in [0, 1], \tag{6.6}$$

so a necessary orientation is $C^{(b)} > u_{thr}(L)/U_L^{(b)}$.

6.2. *Moment bounds from curvature statistics*

The necessary condition expresses fracture in terms of an increment tail evaluated at the mechanical threshold (6.2). To avoid assuming a tail model, we bound $p_{block}(L)$ using only the existence of curvature moments, which also connects directly to refined similarity.

Two classical inequalities will be used (Boucheron, Lugosi & Massart 2013):

$$\mathbb{P}(X > a) \;\leq\; \frac{[X^p]}{a^p}, \qquad X \geq 0,\;\; a > 0,\;\; p > 0 \quad \text{(Markov)}, \tag{6.7}$$

and, for $X \geq 0$ with $0 < \ \ [X] < \infty$ and $\ \ [X^2] < \infty$,

$$\mathbb{P}\big(X > \theta\ \ \ [X]\ \ \geq\; (1-\theta)^2\, \frac{[X]^2}{[X^2]}, \qquad \theta \in (0, 1) \quad \text{(Paley-Zygmund)}. \tag{6.8}$$

Applying (6.7) to $X = \kappa_{blk}^{(b)}$ with $a = \kappa_{frac}$ gives

$$p_{block}(L) \;\leq\; \frac{M_p(L)}{\kappa_{frac}^{p}}, \qquad M_p(L) \equiv \Big\langle\Big(\kappa_{blk}^{(b)}\ \ ^{p}\Big\rangle_b, \quad p > 0. \tag{6.9}$$

Using the intermittency-corrected scaling $M_p(L) \sim (\xi_{\perp}/EI)^p\, \bar{\varepsilon}^{p/3}\, \mathcal{L}^{-\tau(p/3)}\, L^{\gamma_p}$ with $\gamma_p = (7/3)p + \tau(p/3)$ (see (5.6)), or equivalently the moment-based critical span $\ell_c^{(p)}$ defined by $M_p(\ell_c^{(p)}) = \kappa_{frac}^{p}$ ((5.12)), one obtains the compact form

$$p_{block}(L) \lesssim \left(\frac{L}{\ell_c^{(p)}}\right)^{\gamma_p}, \qquad \gamma_p = \frac{7}{3}p + \tau(p/3), \tag{6.10}$$

where $\lesssim$ hides $O(1)$ orientation factors.

For a lower bound, we have already defined $\kappa^{\star}(L) = M_1(L) = \langle\kappa_{blk}^{(b)}\rangle_b > 0$ and $\theta(L) \equiv \kappa_{frac}/\kappa^{\star}(L) \in (0, 1)$. Applying (6.8) with $X = \kappa_{blk}^{(b)}$ yields

$$p_{block}(L) \;\geq\; \frac{\big(1-\theta(L)\ \ ^2\, M_1(L)^2}{M_2(L)} = \frac{\big(1-\theta(L)\ \ ^2}{M_2(L)/M_1(L)^2}. \tag{6.11}$$

With the inertial-range scalings

$$M_1(L) \sim \frac{\xi_\perp}{EI}\,\bar{\varepsilon}^{1/3}\,\mathcal{L}^{-\alpha}\,L^{\,7/3+\alpha}, \qquad M_2(L) \sim \left(\frac{\xi_\perp}{EI}\right)^2 \bar{\varepsilon}^{2/3}\,\mathcal{L}^{-\tau(2/3)}\,L^{\,14/3+\tau(2/3)}, \tag{6.12}$$

(where $\alpha \equiv \tau(1/3)$), the ratio simplifies to

$$\frac{M_2(L)}{M_1(L)^2} \sim \left(\frac{L}{\mathcal{L}}\right)^{\tau(2/3)-2\alpha}, \tag{6.13}$$

and the threshold fraction becomes

$$\theta(L) = \frac{\kappa_{frac}}{M_1(L)} \sim \left(\frac{EI}{\xi_\perp}\right)\bar{\varepsilon}^{-1/3}\,\kappa_{frac}\,\mathcal{L}^{\alpha}\,L^{-\,(7/3+\alpha)}. \tag{6.14}$$

Hence,

$$p_{block}(L) \qquad \big(1-\theta(L)\ ^{2}\left(\frac{L}{\mathcal{L}}\right)^{-\,[\,\tau(2/3)-2\,\tau(1/3)\,]}, \qquad \theta(L)\in(0,\,1). \tag{6.15}$$

This condition of validity ($\kappa_{frac} < \kappa^\star(L)$) marks the supercritical range where exceedances are frequent; once it holds, (6.15) provides a closed L-scaling controlled by intermittency through $\tau(2/3) - 2\tau(1/3)$.

7. Fragmentation cascade: continuous kinetics

7.1. *Subcritical versus supercritical spans: regimes, bounds and hazard*

We sample time in non-overlapping blocks of duration $\Delta T = c\,\tau_L$ with $c = O(1)$ and $\tau_L \sim \bar{\varepsilon}^{-1/3} L^{2/3}$. In each block, a fragment of span L breaks with probability $p_{block}(L) = \mathbb{P}(\kappa^{(b)}_{blk} > \kappa_{frac})$. Let $\mathcal{S}(t)$ be the survival probability up to $t = n\Delta T$. Assuming decorrelation at the block scale, $\mathcal{S}(t) = (1 - p_{block}(L))^n$. By definition of a time-homogeneous hazard $h(L)$, $\mathcal{S}(t) = \exp[-\,h(L)\,t]$. Matching the two expressions at $t = n\Delta T$ yields the exact identity

$$h(L) = \frac{-\ln\!\big(1 - p_{block}(L)\big)}{\Delta T} = \frac{-\ln\!\big(1 - p_{block}(L)\big)}{c\,\tau_L}. \tag{7.1}$$

This simply equates the discrete survival over independent eddy-time ‘trials’ with the continuous-time memoryless survival: $S(n\Delta T) = (1 - p_{block})^n = \exp[-h\,n\Delta T]$. Physically, $p_{block}(L)$ is the probability that at least one curvature-threshold event occurs during one eddy-turnover-time block at scale L, while $h(L)$ is the corresponding mean breakup rate per unit physical time.

Within the inertial subrange, if the hazard is eddy-time-limited, i.e. $h(L) \propto \tau_L^{-1}$, (7.1) yields an $O(1)$ per-block exceedance probability $p_{block}(L) = 1 - \exp[-\,\text{const}]$; this concerns block-level sampling at scale L and does not invoke the unphysical limit $L \to \infty$. Elementary bounds for $-\ln(1-x)$ with $x \in [0,\,1)$ (equivalently, convexity of $-\ln(1-x)$) give

$$\frac{p_{block}(L)}{c\,\tau_L} \le h(L) \le \frac{p_{block}(L)}{(1 - p_{block}(L))\,c\,\tau_L}. \tag{7.2}$$

In the rare-event limit $p_{block}(L) \ll 1$, (7.1) further reduces to $h(L) \simeq p_{block}(L)/(c\,\tau_L)$ up to $O(p_{block})$ corrections, making explicit that on the subcritical branch the hazard is controlled by the small exceedance probability per eddy-time block.

Downloaded from https://www.cambridge.org/core. IP address: 2.34.25.197, on 04 May 2026 at 12:12:30, subject to the Cambridge Core terms of use, available at https://www.cambridge.org/core/terms. https://doi.org/10.1017/jfm.2026.11233

Downloaded from https://www.cambridge.org/core. IP address: 2.34.25.197, on 04 May 2026 at 12:12:30, subject to the Cambridge Core terms of use, available at https://www.cambridge.org/core/terms. https://doi.org/10.1017/jfm.2026.11233

7.1.1. *Subcritical spans* $L < \ell_c^{(1)}$, *i.e.* $y_1(L) < 1$).

In this regime, the typical block-peak curvature lies below threshold ($\kappa^\star < \kappa_{frac}$) and fracture requires rare fluctuations, hence $p_{block}(L) \ll 1$. In this rare-event limit, (7.1) linearises to $h(L) \simeq p_{block}(L)/(c\,\tau_L)$ when $p_{block} \ll 1$. Markov's inequality on $\kappa_{blk}^{(b)}$ gives $p_{block}(L) \le y_1(L)$ since $p_{block}(L) = \mathbb{P}(\kappa_{blk}^{(b)} > \kappa_{frac}) \le \langle \kappa_{blk}^{(b)} \rangle_b / \kappa_{frac} = M_1(L)/\kappa_{frac} = y_1(L)$. Physically, $y_1(L) < 1$ means that a typical eddy-time forcing bends the fibre below its fracture curvature, so breakup is controlled by rare tail events rather than by the mean load. Combining with (7.1)–(7.2) yields

$$h(L) \;\le\; \frac{-\ln\big(1 - y_1(L)}{c\,\tau_L} \;\le\; \frac{y_1(L)}{(1 - y_1(L))\,c\,\tau_L}. \tag{7.3}$$

Using $\tau_L \sim \bar{\varepsilon}^{-1/3} L^{2/3}$ together with the inertial-range scaling of M_1 gives the estimate

$$h(L) \;\lesssim\; C_1\,\frac{\xi_\perp}{E I\,\kappa_{frac}}\,\bar{\varepsilon}^{2/3}\,\mathcal{L}^{-\alpha}\,L^{\,5/3+\alpha}, \tag{7.4}$$

where $C_1 = O(1)$ incorporates the orientation factor and c^{-1}. Paley–Zygmund bound does not apply here because $\theta(L) > 1$.

7.1.2. *Supercritical spans* $L > \ell_c^{(1)}$, *i.e.* $y_1(L) > 1$).

When the typical curvature exceeds the material threshold ($\kappa^\star > \kappa_{frac}$), exceedances within an eddy-time block are not rare: $p_{block}(L) = O(1)$. Here $y_1(L) > 1$ means that a typical eddy-time block already samples curvatures at/above threshold, so the breakup 'clock' is set by the eddy turnover at scale L. Writing $y_1(L) \equiv \kappa^\star(L)/\kappa_{frac} > 1$ and $\theta(L) = 1/y_1(L) \in (0, 1)$, Paley–Zygmund applied to the block peak $\kappa_{blk}^{(b)}$ gives

$$p_{block}(L) \;\ge\; \frac{\big(1 - \theta(L)\;{}^{2}\,M_1(L)^2}{M_2(L)} \;=\; \frac{\big(1 - 1/y_1(L)\;{}^{2}}{M_2(L)/M_1(L)^2}. \tag{7.5}$$

The ratio $C_2(L) \equiv M_2(L)/M_1(L)^2$ is a normalised-moment ratio and remains $O(1)$ in the inertial range (under refined similarity it does not introduce additional powers of L); hence, for any $y_1(L) > 1$, the right-hand side is strictly positive, and as $y_1 \to \infty$ it approaches a branch-dependent constant <1 (namely $1/C_2$).

The hazard follows from the block relation $h(L) = [-\ln(1 - p_{block}(L))]/(c\,\tau_L)$, with $\tau_L \sim \bar{\varepsilon}^{-1/3} L^{2/3}$ and $c = O(1)$. Using $x \le -\ln(1 - x) \le x/(1 - x)$ for $x \in (0, 1)$,

$$\frac{p_{block}^{(\mathrm{lb})}(L)}{c\,\tau_L} \;\le\; h(L) \;\le\; \frac{p_{block}(L)}{(1 - p_{block}(L))\,c\,\tau_L}, \tag{7.6}$$

where (lb) stands for 'lower bound'. The Paley–Zygmund lower bound thus yields a quantitative floor $h(L)$ $\quad$ const $\tau_L^{-1} = O(\bar{\varepsilon}^{1/3} L^{-2/3})$. In contrast, Markov's inequality supplies only $p_{block} \le M_p/\kappa_{frac}^p$; for $p = 1$ this is $p_{block} \le y_1 > 1$ (clipped to 1), and for $p \ge 2$ it scales like $C_2\,y_1^p \ge 1$, so it becomes non-informative above threshold.

In summary, for $L < \ell_c^{(1)}$, Markov's inequality gives the upper bound $h(L) \lesssim C\,L^{5/3+\alpha}$. As a closure, we assume bound saturation up to order-one factors and simply take $h(L) \propto L^{5/3+\alpha}$ on the subcritical branch; the proportionality constant will be introduced later when specifying the hazard law. For $L > \ell_c^{(1)}$, the process is eddy-time-limited, $h(L) = O(1/\tau_L)$, with a strictly positive lower bound from Paley–Zygmund.

Downloaded from https://www.cambridge.org/core. IP address: 2.34.25.197, on 04 May 2026 at 12:12:30, subject to the Cambridge Core terms of use, available at https://www.cambridge.org/core/terms. https://doi.org/10.1017/jfm.2026.11233

Let us conclude this section with a comparison with the fragmentation results of Brouzet *et al.* (2021). Our hazard $h(L)$ is a physical rate defined by (7.1) with block length $\Delta T = c\,\tau_L$. In Brouzet *et al.* (2021), the breaking probability $p(L)$ is inferred from curvature statistics and made extensive in L by treating a long fibre as L independent elastic-length pieces; their kinetic equation (their equation (18)) uses a model time scale that, as stated by the authors, cannot be related to any physical quantity, and a mapping to physical time is provided only for the numerical tails (their figure 5*c*), while the experiments do not show a linear-in-time scaling. For these reasons, we do not attempt a rate-to-rate fit; instead we compare structural signatures: (i) the strong decrease of breaking probability for short L and the minimal fragment length near $L \approx 1$ (their figure 4*a*), consistent with our critical span and rare-event branch; (ii) for large L, differences expected from distinct closures (their extensive $p(L)$ versus our eddy-time-limited $h(L) \propto \tau_L^{-1}$).

7.2. *Fragmentation operator and kinetic equation with sources and sinks*

The population-balance description of fragmentation processes has a long tradition in chemical and environmental engineering, as reviewed for instance by Hulburt & Katz (1964), Ramkrishna (2000), and rigorously developed in the mathematical literature on coagulation–fragmentation equations (e.g. Ziff & McGrady 1985; Escobedo *et al.* 2005; Bertoin 2006; Banasiak *et al.* 2019). Let $n(L,t)$ be the number density (per unit L). On breakage of a parent of length L_p, the daughter-length intensity is described by a kernel $B(L \mid L_p)$ with units 1/length, defined so that the expected number of daughters in $[L, L+\mathrm{d}L]$ is $B(L \mid L_p)\,\mathrm{d}L$ for $0 < L < L_p$. This is the standard daughter distribution kernel used in population-balance equations for droplet and aggregate breakup (e.g. Bäbler *et al.* 2008; Babler *et al.* 2015).

With hazard $h(L)$ from (7.1), the loss at size L is $h(L)\,n(L,t)$; the gain is the contribution from larger parents breaking into daughters of size L. To include environmental inputs/removal, we add a source $S(L,t) \geq 0$ and a sink $Q(L) \geq 0$, as is standard in environmental transport models (see e.g. Ramkrishna 2000). The kinetic equation then reads

$$\partial_t n(L,t) = -\underbrace{h(L)\,n(L,t)}_{\text{loss by breakage}} + \underbrace{\int_L h(L_p)\,n(L_p,t)\,B(L \mid L_p)\,\mathrm{d}L_p}_{\text{gain from larger parents}} + \underbrace{S(L,t)}_{\text{external input}} - \underbrace{Q(L)\,n(L,t)}_{\text{removal (sink)}}. \tag{7.7}$$

We take $L \in (L_{min}, \mathcal{L}]$. The upper bound $\mathcal{L}$ is the largest admissible parent size. Small-size removal can be implemented either as an absorbing boundary at $L_{min} > 0$ (then $Q \equiv 0$ on $(L_{min}, \mathcal{L}]$) or as a bulk sink $Q(L) > 0$ increasing toward small L. Such sink terms are widely used to represent physical removal by deposition, filtration or beaching (e.g. Ramkrishna 2000; Doumic, Escobedo & Tournus 2018). Typical inputs are monodisperse, $S(L,t) = J(t)\,\delta(L - \mathcal{L})$ here $J(t)$ is the prescribed injection flux (number of fibres injected per unit time and unit volume) at the parent size $\mathcal{L}$, or distributed sources over large sizes, as in environmental fragmentation cascades of aggregates and fibres (Andrady 2011; Kalogerakis *et al.* 2017; Suaria *et al.* 2020).

Number and length constraints on B are (see, e.g. Ziff & McGrady 1985; Bertoin 2006; Bäbler *et al.* 2008; Babler *et al.* 2015):

$$K(L_p) = \int_0^{L_p} B(L \mid L_p)\,\mathrm{d}L, \qquad \int_0^{L_p} L\,B(L \mid L_p)\,\mathrm{d}L = L_p, \tag{7.8}$$

Downloaded from https://www.cambridge.org/core. IP address: 2.34.25.197, on 04 May 2026 at 12:12:30, subject to the Cambridge Core terms of use, available at https://www.cambridge.org/core/terms. https://doi.org/10.1017/jfm.2026.11233

so that $K(L_p)$ is the expected multiplicity while total length is conserved at each break. These balance conditions are the direct analogue of mass conservation in aggregate and droplet breakup models (e.g. Bäbler *et al.* 2008; Villermaux 2007).

7.3. *Freely decaying case: a self-similar binary kernel*

We now set $S \equiv 0$ and $Q \equiv 0$ and consider $L \in (0, \mathcal{L}]$. The Kolmogorov scale $\eta \sim (\nu^3/\bar{\varepsilon})^{1/4}$ (Frisch 1995) marks the onset of a smooth viscous subrange, where ν is the kinematic viscosity of the carrier fluid; for $L \lesssim \eta$ (Allende *et al.* 2018, 2020), the hazard is expected to be very small and the flux toward vanishing sizes negligible on observational times. We nevertheless keep 0 for the formal lower bound; all integrals are well defined if $n(\ \ , t)$ is integrable at 0^+.

When a parent of length L_p breaks into two daughters, set the shrinkage $r \equiv L_{dau}/L_p \in (0, 1)$, where L_{dau} denotes a daughter (fragment) length produced by the breakup of a parent of length L_p and let $\rho(r)$ be an exchange-symmetric probability density function (p.d.f.), $\rho(r) = \rho(1 - r)$, normalised on (0, 1). A convenient scale-invariant binary kernel is (e.g. Ziff & McGrady 1985; McGrady & Ziff 1987; Bertoin 2006)

$$B(L \mid L_p) = \frac{2}{L_p}\, \rho\left(\frac{L}{L_p}\right), \qquad 0 < L < L_p, \tag{7.9}$$

which satisfies (7.8) with $K \equiv 2$ and exact length conservation by symmetry. In the small-slope, bending-dominated regime underlying the present load-to-curvature map, the curvature peak is typically attained near midspan, so breakup is expected to be predominantly quasi-central; accordingly, in what follows we interpret $\rho(r)$ as concentrated around $r = 1/2$ (with negligible weight near $r \to 0$ or 1), while keeping the scale-invariant form (7.9) for notational generality. By contrast, impact-driven fragmentation of slender brittle rods can involve dynamic buckling and bending-wave effects, leading to different daughter-size statistics and possibly multiple secondary breaks (Vandenberghe & Villermaux 2013).

Multiplying (7.7) by L^k and integrating over L, Tonelli's theorem (Banasiak *et al.* 2019) justifies exchanging the order of integration in the gain term and yields the moment balance

$$\dot{m}_k(t) = \int_0 \ \ h(L)\, n(L, t)\, \big(\beta_k(L) - 1 \ \ L^k\, \mathrm{d}L, \qquad \beta_k(L) \equiv \frac{1}{L^k} \int_0^L \ \ ^k\, B(\ \ \mid L)\, \mathrm{d}\ \ . \tag{7.10}$$

For the kernel (7.9), $\beta_k = 2\,\langle r^k \rangle_\rho$ is constant, so

$$\begin{aligned} &\dot{m}_1 = 0 && \text{(length conserved)} \\ &\dot{m}_0 = \int h\, n\, \mathrm{d}L > 0 && \text{(fragment count grows)} \\ &\dot{m}_k < 0, \qquad k > 1 && \text{(higher moments decrease).} \end{aligned} \tag{7.11}$$

A succinct derivation of (7.10) and the convexity argument for $k > 1$ are deferred to Appendix B.

7.4. *Self-similar description, typical size and fixed-shape equation*

Self-similar formulations are natural in fragmentation kinetics, since both theory and experiments show that fragment-size distributions evolve toward scaling profiles under broad conditions (e.g. Ziff & McGrady 1985; McGrady & Ziff 1987; Leyvraz 2003; Bertoin 2006; Villermaux 2007). For a recent perspective contrasting principle-based and mechanism-based views of fragmentation statistics, and discussing the emergence

Downloaded from https://www.cambridge.org/core. IP address: 2.34.25.197, on 04 May 2026 at 12:12:30, subject to the Cambridge Core terms of use, available at https://www.cambridge.org/core/terms. https://doi.org/10.1017/jfm.2026.11233

(and limitations) of power-law fragment-size distributions under maximal-randomness arguments, see Villermaux (2025).

Physically, this reflects the absence of any intrinsic length scale in the binary breakup kernel: once the typical size $L_*(t)$ is factored out, the fragment distribution collapses onto a stationary shape $F(x)$ when expressed in terms of the rescaled variable $x = L/L_*(t)$. In other words, the cascade proceeds by a continual shift of the typical length, while the normalised profile remains statistically invariant. We therefore introduce the similarity representation

$$n(L,t) \equiv \quad (t)\, F(x)\,, \qquad x \equiv \frac{L}{L_*(t)}, \qquad L_*(t) \equiv \frac{m_1(t)}{m_0(t)}, \tag{7.12}$$

with the length-preserving normalisation $\int_0^{x_{max}(t)} x\, F(x)\, \mathrm{d}x = 1$, where $x_{max}(t) = \mathcal{L}/L_*(t)$. This choice implies $\quad (t) = L_*(t)^{-2}$ and $m_0(t) = L_*^{-1} \int_0^{x_{max}} F(x)\, \mathrm{d}x$. Note that $L_*(t) = m_1(t)/m_0(t)$ is the mean fragment length; its time evolution is an experimentally accessible observable that can be confronted (only qualitatively) with mean-length curves reported in laboratory/numerical studies (e.g. Brouzet *et al.* 2021). A point-by-point quantitative overlay would require specifying the corresponding $O(1)$ prefactors in the hazard (and, in experiments, the statistics of the breaking threshold), which are set-up-dependent and not constrained in the present scaling treatment.

A mean-lineage argument shows that the geometric typical size satisfies

$$\frac{d}{\mathrm{d}t} \ln L_*(t) = -\, c_{eff}\, h\big(L_*(t) \;\;, \qquad c_{eff} \equiv \quad [-\ln r] > 0, \tag{7.13}$$

which integrates to

$$\int_{L_*(t)}^{L_*(0)} \frac{\mathrm{d}\ell}{\ell\, h(\ell)} = c_{eff}\, t. \tag{7.14}$$

It is convenient to non-dimensionalise time with the integral (large-eddy) turnover time at $\mathcal{L}$, i.e. $T_0 \equiv \tau \quad \sim \bar{\varepsilon}^{-1/3} \mathcal{L}^{2/3}$, and to consider the trajectory $L_*(t)/\mathcal{L}$ as a function of t/T_0. Figure 1 shows illustrative mean-length trajectories obtained by integrating (7.13) with the two inertial-range hazard branches (eddy-time-limited for $L > \ell_c$ and rare-event for $L < \ell_c$), for different values of $\ell_c/\mathcal{L}$ (mimicking different breaking thresholds).

The short proof (Poisson clock at rate $h(L_*)$ and multiplicative shrinkage r) and the equivalence with the arithmetic definition m_1/m_0 up to a time-independent factor are given in Appendix C.

For a power-law hazard $\quad h(L) = K\, L^{\beta}$, substituting $-\dot{L}_*/L_* = c_{eff} K\, L_*^{\beta}$ into the similarity form of (7.7) with the kernel (7.9) eliminates explicit time dependence and yields the fixed-shape equation

$$c_{eff}\,(2F + xF') \;+\; x^{\beta} F(x) = \underbrace{\int_x^{\infty} y^{\beta-1} F(y)\, 2\, \rho\left(\frac{x}{y}\right)\, \mathrm{d}y}_{\text{gain integral}}, \qquad x > 0, \tag{7.15}$$

with $\int_0^{\infty} x F = 1$. Technical steps (change of variables, support truncation $x_{max} \gg 1$, and the autonomous limit) are summarised in Appendix D.

Downloaded from https://www.cambridge.org/core. IP address: 2.34.25.197, on 04 May 2026 at 12:12:30, subject to the Cambridge Core terms of use, available at https://www.cambridge.org/core/terms. https://doi.org/10.1017/jfm.2026.11233

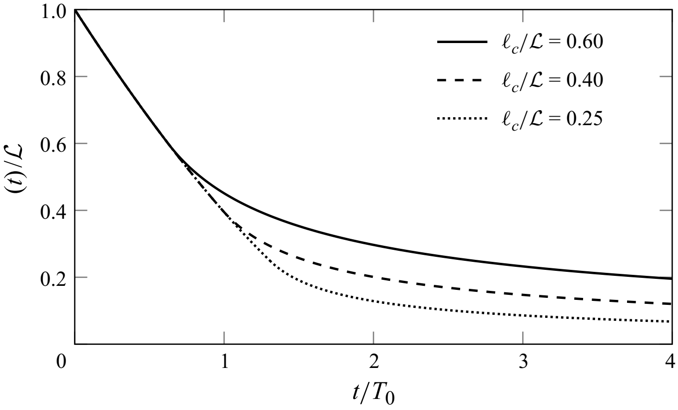

Figure 1. Illustrative evolution of the mean fragment length $L_*(t) = m_1(t)/m_0(t)$ predicted by (7.13) (equivalently (7.14)), shown as $L_*(t)/$ versus t/T_0 with $T_0 \equiv \tau \quad \sim \bar{\varepsilon}^{-1/3} \quad {}^{2/3}$. The curves are obtained by integrating (7.13) using a two-branch inertial-range hazard: $h \propto L^{-2/3}$ for $L > \ell_c$ (eddy-time-limited) and $h \propto L^{5/3}$ for $L < \ell_c$ (rare-event; here $\alpha = 0$ for simplicity). Different values of $\ell_c/$ mimic different breaking thresholds ('brittleness';) as in Brouzet *et al.* 2021. All $O(1)$ prefactors are set to unity, hence the plot is meant as a qualitative comparison rather than a quantitative fit.

7.5. *Start-up time to the critical span*

The time to decrease from $L_*(0) \approx \mathcal{L}$ to a target size L_{tgt} follows from (7.14):

$$t\big(\mathcal{L}\to L_{tgt} \quad = \frac{1}{c_{eff}} \int_{L_{tgt}} \frac{\mathrm{d}\ell}{\ell\, h(\ell)}. \tag{7.16}$$

Along the supercritical branch ($L \downarrow \ell_c^{(1)}$), the hazard is eddy-time limited, $h(L) = \kappa_h\, \bar{\varepsilon}^{1/3} L^{-2/3}$ with $\kappa_h = O(1)$, giving

$$t\big(\mathcal{L}\to \ell_c^{(1)} \quad \simeq \frac{3}{2\, c_{eff}\, \kappa_h}\, \bar{\varepsilon}^{-1/3} \left(\mathcal{L}^{2/3} - \ell_c^{2/3}\right), \tag{7.17}$$

and the mean-field closed form upon substituting $\ell_c = (\kappa_{frac} EI/(\xi_\perp\, \bar{\varepsilon}^{1/3}))^{3/7}$:

$$t\big(\mathcal{L}\to \ell_c \quad \simeq \frac{3}{2\, c_{eff}\, \kappa_h}\, \bar{\varepsilon}^{-1/3} \left[\mathcal{L}^{2/3} - \left(\frac{\kappa_{frac}\, EI}{\xi_\perp\, \bar{\varepsilon}^{1/3}}\right)^{2/7}\right]. \tag{7.18}$$

Here $c_{eff} = \quad [-\ln r]$ is an $O(1)$ constant set by the daughter-ratio p.d.f. $\rho(r)$ (for an ideal central split $r \equiv 1/2$, $c_{eff} = \ln 2$), while $\kappa_h = O(1)$ is the eddy-time-limited prefactor in $h(L) = \kappa_h\, \bar{\varepsilon}^{1/3} L^{-2/3}$ (equivalently $h = \kappa_h/\tau_L$). Combining this closure with the block identity (7.1) (with $\Delta T = c\, \tau_L$) shows that κ_h can be interpreted as the dimensionless log-survival decrement per eddy-time block in the supercritical range, $-\ln(1 - p_{block}) = c\, \kappa_h$; in the present scaling treatment, we leave both prefactors unspecified since they affect only the amplitudes of the time scales.

7.6. *Subcritical branch: halving time and slow-down below ℓ_c*

Below $\ell_c^{(1)}$, exceedances are rare and the hazard increases with size. We model $h(L) = K_{sub}\, L^{\beta}$ with $\beta > 0$; in our prototype $\beta = 5/3 + \alpha$ and

$$K_{sub} = \kappa_{sub}\, \frac{\xi_\perp}{EI\, \kappa_{frac}}\, \bar{\varepsilon}^{2/3}\, \mathcal{L}^{-\alpha}, \qquad \kappa_{sub} = O(1). \tag{7.19}$$

Downloaded from https://www.cambridge.org/core. IP address: 2.34.25.197, on 04 May 2026 at 12:12:30, subject to the Cambridge Core terms of use, available at https://www.cambridge.org/core/terms. https://doi.org/10.1017/jfm.2026.11233

Using (7.16) (i.e. $t(L_1 \to L_2) = (1/c_{eff}) \int_{L_2}^{L_1} (\mathrm{d}\ell/\ell\, h(\ell))$ along a typical lineage) between L_1 and $L_2 < L_1$ gives

$$t(L_1 \to L_2) = \frac{1}{c_{eff} K_{sub}\, \beta} \left(L_2^{-\beta} - L_1^{-\beta} \right), \tag{7.20}$$

and the halving time

$$t_{1/2}(L) \ = \ t(L \to L/2) = \frac{2^{\beta} - 1}{c_{eff}\, K_{sub}\, \beta}\, L^{-\beta}. \tag{7.21}$$

With $\beta = 5/3 + \alpha$ this becomes

$$t_{1/2}(L) = \frac{2^{\,5/3+\alpha} - 1}{(5/3+\alpha)\, c_{eff}\, \kappa_{sub}} \left(\frac{EI\, \kappa_{frac}}{\xi_\perp} \right) \bar{\varepsilon}^{-2/3}\, \mathcal{L}^{\alpha}\, L^{-\,(5/3+\alpha)}. \tag{7.22}$$

An equivalent form in terms of ℓ_c is

$$t_{1/2}(L) = \frac{2^{\beta} - 1}{\beta\, c_{eff}\, \kappa_{sub}}\, \tau_L(\ell_c) \left(\frac{\ell_c}{L} \right)^{\beta}, \qquad \beta = 5/3 + \alpha, \quad \tau_L(L) = \bar{\varepsilon}^{-1/3} L^{2/3}, \tag{7.23}$$

showing that $t_{1/2}(L)$ increases sharply as L decreases: there is no finite-time collapse below ℓ_c. Indeed, for $\beta > 0$ one has $t_{1/2}(L) \propto L^{-\beta} \to \infty$ as $L \downarrow 0$: physically, below ℓ_c the typical curvature falls further below κ_{frac}, so breakage is controlled by increasingly rare bursts rather than by an eddy-time clock.

It is also useful to compute the time required for the typical size to decrease from the critical span ℓ_c down to the Kolmogorov scale η. This follows by integrating the inverse hazard rate $h(L)^{-1}$ across the subcritical branch, yielding

$$t(\ell_c \to \eta) = \frac{1}{\beta\, c_{eff}\, K_{sub}} \left(\eta^{-\beta} - \ell_c^{-\beta} \right. = \frac{1}{\beta\, c_{eff}\, \kappa_{sub}}\, \tau_L(\ell_c) \left(\frac{\ell_c}{\eta} \right)^{\beta}, \qquad \beta = 5/3 + \alpha, \tag{7.24}$$

where $\tau_L(L) = \bar{\varepsilon}^{-1/3} L^{2/3}$. For $\eta \ll \ell_c$, this asymptotic form demonstrates that the descent towards the dissipative scale is progressively slowed down.

To make parameter dependences explicit, we substitute the mean-field expressions $\ell_c = (\kappa_{frac} EI/(\xi_\perp \bar{\varepsilon}^{1/3}))^{3/7}$ and $\eta = (\nu^3/\bar{\varepsilon})^{1/4}$ into (7.24). This yields the compact scaling

$$t(\ell_c \to \eta) \simeq \frac{1}{\beta\, c_{eff}\, \kappa_{sub}} \left(\frac{\kappa_{frac}\, EI}{\xi_\perp} \right) \nu^{-\frac{3\beta}{4}}\, \bar{\varepsilon}^{\frac{3\beta - 8}{12}}\, \mathcal{L}^{\alpha}, \qquad \beta = 5/3 + \alpha, \tag{7.25}$$

up to $O(1)$ shape/orientation factors in $\xi_\perp$. For a circular section, $I = \pi a^4/4$ and $\xi_\perp \simeq 4\pi\mu/(\ln \quad + \delta_\perp)$ with $\quad = L/a \gg 1$ (evaluated at $L \simeq \ell_c$).

(i) The dependence on fibre geometry/material is strong: since $EI \propto a^4$, one has $t \propto a^3$ up to a weak logarithmic correction from $\xi_\perp$. Moreover t is linear in κ_{frac}. (ii) The dependence on viscosity is strong, $t \propto \nu^{-3\beta/4}$, together with an additional linear factor μ^{-1} hidden in $\xi_\perp$. (iii) The dependence on mean dissipation is comparatively weak, $t \propto \bar{\varepsilon}^{(3\beta-8)/12}$ (for $\beta \simeq 5/3$, $t \propto \bar{\varepsilon}^{-1/4}$). (iv) The drag coefficient $\xi_\perp$ contributes only through a mild (logarithmic) variation with a and , but also carries the inverse viscosity dependence mentioned in (ii). Intermittency enters via $\beta = 5/3 + \alpha$, introducing the explicit prefactor $\mathcal{L}^{\alpha}$ and slightly modifying the exponents, without altering the qualitative hierarchy of sensitivities.

Downloaded from https://www.cambridge.org/core. IP address: 2.34.25.197, on 04 May 2026 at 12:12:30, subject to the Cambridge Core terms of use, available at https://www.cambridge.org/core/terms. https://doi.org/10.1017/jfm.2026.11233

7.7. *Similarity-profile asymptotics*

In the deep-cascade regime ($L_* \ll \mathcal{L}$), the fixed-shape problem (7.15) admits clean small- and large-x asymptotics that depend only on β and on the behaviour of ρ near $r = 0, 1$.
Small x. For $\beta > 0$ (rare-event branch), $x^\beta F(x) \to 0$ and $\rho(x/y) \to \rho(0)$ inside the gain integral in (7.15), so the right-hand side approaches a finite constant

$$\quad := 2\rho(0) \int_0^\infty y^{\beta-1} F(y)\,\mathrm{d}y \in (0, \infty). \tag{7.26}$$

Writing $G(x) := x^2 F(x)$, note that $2F + xF' = (1/x)G'(x)$. Hence (7.15) yields $c_{\mathit{eff}}(1/x)G'(x) = \quad + o(1)$ as $x \downarrow 0$, i.e. $G'(x) = (\;\;/c_{\mathit{eff}})x + o(x)$. Integrating gives $G(x) = (\;\;/2c_{\mathit{eff}})x^2 + o(x^2)$, and therefore

$$F(x) = F(0) + O(x^2), \qquad F(0) = \frac{}{2c_{\mathit{eff}}} > 0. \tag{7.27}$$

For $\beta < 0$ (eddy-time-limited branch), a dominant balance between $x^\beta F$ and the gain term fixes a power-law depletion $F(x) \sim C\,x^\mu$ with $\mu = m - \beta > 0$ if $\rho(r) \sim c_m r^m$ as $r \downarrow 0$ (near-central splitting). These small-x limits follow from a standard dominant-balance expansion of (7.15) as $x \downarrow 0$; see e.g. Ziff & McGrady (1985), Escobedo *et al.* (2005).
Large x. If $\beta > 0$, the dominant balance is the homogeneous transport-reaction ordinary differential equation $c_{\mathit{eff}}(2F + xF') + x^\beta F = 0$, giving the stretched-exponential tail

$$F(x) \sim C_\infty\, x^{-2} \exp\left(-\frac{x^\beta}{\beta\, c_{\mathit{eff}}}\right) \qquad (x \to \infty). \tag{7.28}$$

where C_∞ is a positive constant prefactor. If $\beta < 0$, $x^\beta \to 0$ and the leading tail is $F(x) \sim C_-\,x^{-2}(1 + O(x^\beta))$. These large-$x$ tails follow from the leading-order balance of (7.15) as $x \to \infty$; see e.g. Ziff & McGrady (1985), Bertoin (2006).
Branch-aware interpretation. In the similarity variable $x \equiv L/L_*(t)$, 'large-x' must be read within the active hazard branch. Let $x_c(t) \equiv \ell_c^{(1)}/L_*(t)$. For $\beta > 0$ (valid for $L < \ell_c^{(1)}$), the tail applies on $1 \ll x \ll x_c(t)$ and matches to the $\beta < 0$ tail for $x \gg x_c(t)$; for early times $x_c < 1$, only the $\beta < 0$ tail is sampled.

Summarising, (i) the decay law for $L_*(t)$ is fixed by $h(\;)$ via (7.14), hence by turbulence through p_{block} and τ_L. (ii) For $L_* \ll \mathcal{L}$, histograms of L collapse under $L \mapsto L/L_*(t)$ onto the fixed profile F. (iii) The outer-tail rate $1/(\beta c_{\mathit{eff}})$ diagnoses the hazard exponent and the daughter-ratio dispersion, connecting fragmentation statistics to both turbulent forcing and splitting physics.

7.8. *Bulk power-law scaling in steady-state fragmentation*

In the stationary regime, the population balance (7.7) with the binary self-similar kernel (7.9) reads

$$0 = -h(L)\,n(L) + \int_L h(L_p)\,n(L_p)\,B(L \mid L_p)\,\mathrm{d}L_p + S(L,t) - Q(L)\,n(L). \tag{7.29}$$

In the inertial bulk, we assume negligible local support of input and sink,

$$L_{min} \ll L \ll \mathcal{L}, \qquad S(L,t) \simeq 0, \qquad Q(L) \simeq 0, \tag{7.30}$$

so that (7.29) reduces to

$$h(L)\,n(L) = \int_L h(L_p)\,n(L_p)\,\frac{2}{L_p}\,\rho\left(\frac{L}{L_p}\right)\,\mathrm{d}L_p. \tag{7.31}$$

Assume a single hazard branch governs the bulk and seek a power law

$$h(L) = K\,L^{\beta}, \qquad n(L) = C\,L^{-\tau}. \tag{7.32}$$

Substituting (7.32) into (7.31) and setting $r = L/L_p$ yields

$$1 = 2\int_0^1 r^{\,\tau-\beta-1}\,\rho(r)\,\mathrm{d}r. \tag{7.33}$$

Because $\rho(r) = \rho(1-r)$, we have $\quad [r] = 1/2$; since $2\int_0^1 r^{\,s}\rho(r)\,\mathrm{d}r$ is strictly decreasing in s, the unique solution is $s = 1$ from which we have

$$\tau = \beta + 2. \tag{7.34}$$

7.9. *Horizontal-convergence removal: model, rationale and scaling*

In § 7.8 we have derived the bulk power laws assuming no removal across the vertical boundaries of the sampled layer. Here we make removal explicit and, motivated by ocean surface kinematics, focus on breakup events occurring near horizontal-convergence lines, where the same kinematics that promotes breakup also induces downwelling/subduction and can remove a fraction of daughters. We capture this with a bulk-constant retention $q \in (0,\,1]$ in (7.31). Namely,

$$h(L)\,n(L) = \int_L h(L_p)\,n(L_p)\,\frac{2\,q}{L_p}\,\rho\left(\frac{L}{L_p}\right)\,\mathrm{d}L_p. \tag{7.35}$$

With the single-branch ansatz $h(L) = KL^{\beta}$, $n(L) = CL^{-\tau_q}$ where τ_q is the exponent of the steady power-law distribution with retention q and $r = L/L_p$, one obtains the moment condition

$$1 = 2q\int_0^1 r^{\,\tau_q-\beta-1}\,\rho(r)\,\mathrm{d}r. \tag{7.36}$$

Let $S \equiv \tau_q - \beta - 1$. Then S is determined by

$$\mathcal{M}(S) \;\equiv\; 2\int_0^1 r^{\,S}\rho(r)\,\mathrm{d}r = \frac{1}{q}, \qquad \text{with } \mathcal{M}(1) = 1 \text{ (length conservation).} \tag{7.37}$$

For quasi-central binary kernels, $\mathcal{M}(S) \simeq 2^{\,1-S}$ and (7.37) gives the compact result

$$\begin{gathered} S = 1 + \log_2 q, \\ \tau_q = \beta + 2 + \log_2 q\,. \end{gathered} \tag{7.38}$$

Two reference cases follow immediately:

$$q = 1 \text{ (no removal, recovers §7.8)} \qquad \Rightarrow\; \tau_1 = \beta + 2, \tag{7.39}$$

$$q = \frac{1}{2} \text{ (on average, one of the two daughters is removed)} \qquad \Rightarrow\; \tau_{1/2} = \beta + 1. \tag{7.40}$$

Here $q = 1/2$ is used as a symmetry-based benchmark consistent with convergence-line removal (on average, one daughter is exported and one is retained); no tuning of q was performed when comparing exponents to observations. Note that the $q = 1/2$ scaling behaviour is shallower than that of $q = 1$ ($\tau_{1/2} = \beta + 1 < \tau_1 = \beta + 2$). Removal thus exports a fraction of daughters before they can fragment further, weakening the forward cascade toward small sizes and leaving relatively more weight at larger L.

Downloaded from https://www.cambridge.org/core. IP address: 2.34.25.197, on 04 May 2026 at 12:12:30, subject to the Cambridge Core terms of use, available at https://www.cambridge.org/core/terms. https://doi.org/10.1017/jfm.2026.11233

Downloaded from https://www.cambridge.org/core. IP address: 2.34.25.197, on 04 May 2026 at 12:12:30, subject to the Cambridge Core terms of use, available at https://www.cambridge.org/core/terms. https://doi.org/10.1017/jfm.2026.11233

7.10. *Amplitude and length flux with removal*

Let $\Pi_1 \equiv \int_0 \; L\, S(L,t)\, \mathrm{d}L$ be the stationary injection of the conserved length moment. We now compute the local downscale flux of length through scale L in a thin logarithmic bin. Set $\xi \equiv \ln L$ and consider the shell $[\xi, \xi + \Delta\xi]$ with $\Delta\xi \ll 1$ (so $\mathrm{d}L = L\,\mathrm{d}\xi$). The number of parents in the shell is $n(L)\,\mathrm{d}L = n(L)\,L\,\Delta\xi$, and the breakage events per unit time are

$$\text{events} = h(L)\,n(L)\,L\,\Delta\xi. \tag{7.41}$$

With retention q (§ 7.9), the *expected* in-layer daughter length that crosses the lower edge of the shell for one such event (parent length L) is

$$\Delta\mathcal{L}_q = 2q\int_0^1 (rL)\,\rho(r)\,\mathbf{1}\{rL < L\}\,\mathrm{d}r = \Lambda_1(q)\,L, \qquad \Lambda_1(q) \equiv 2q\int_0^1 r\,\rho(r)\,\mathrm{d}r, \tag{7.42}$$

where $\mathbf{1}\{rL < L\}$ is the indicator function, which is 1 if the condition is true and 0 otherwise. Consequently, the flux of length across L per unit time and per unit ξ is

$$ {}_q(L) \equiv \lim_{\Delta\xi\to 0} \frac{\text{events} \quad \Delta\mathcal{L}_q}{\Delta\xi} = \Lambda_1(q)\,h(L)\,n(L)\,L^2. \tag{7.43}$$

For symmetric splits, $\int_0^1 r\,\rho(r)\,\mathrm{d}r = 1/2$, hence $\Lambda_1(q) = q$.

With the bulk ansatz $h(L) = K L^{\beta}$ and $n(L) = C\,L^{-\tau_q}$ and using $\tau_q = \beta + 2 + \log_2 q$ (§ 7.9, quasi-central kernel), (7.43) gives

$$ {}_q(L) = \Lambda_1(q)\,K\,C\,L^{\beta+2-\tau_q} = \Lambda_1(q)\,K\,C\,L^{-\log_2 q}. \tag{7.44}$$

Thus the downscale length flux is L-independent only for $q = 1$; for $q < 1$ it decreases toward small L as $L^{-\log_2 q}$.

Amplitudes in two reference cases.

(i) $q = 1$ (no removal). Then $\Lambda_1(1) = 1$ and ${}_1(L) \equiv \Pi_1$ is constant, so

$$n(L) = \frac{\Pi_1}{K}\,L^{-(\beta+2)}, \qquad L_{min} \ll L \ll \mathcal{L}. \tag{7.45}$$

(ii) $q = 1/2$ (on average, one of the two daughters is removed). Here $\Lambda_1(1/2) = 1/2$ and ${}_{1/2}(L) = (1/2)KC\,L$. Let $\Pi_1^{\downarrow} \equiv \lim_{\varepsilon\to 0^+} \; {}_{1/2}(\mathcal{L} - \varepsilon)$ be the top-of-cascade in-layer flux just below $\mathcal{L}$. Then

$$C = \frac{2\,\Pi_1^{\downarrow}}{K\,\mathcal{L}}, \qquad \Rightarrow \qquad n(L) = \frac{2\,\Pi_1^{\downarrow}}{K\,\mathcal{L}}\,L^{-(\beta+1)}, \qquad L_{min} \ll L \ll \mathcal{L}. \tag{7.46}$$

7.10.1. *Scaling law in the subcritical bulk*

On the subcritical branch the hazard is

$$h(L) = K_{sub}\,L^{\beta_{sub}}, \qquad \beta_{sub} = 5/3 + \alpha, \qquad K_{sub} = \kappa_{sub}\,\frac{\xi_{\perp}}{EI\,\kappa_{frac}}\,\bar{\varepsilon}^{2/3}\,\mathcal{L}^{-\alpha}, \tag{7.47}$$

with $\kappa_{sub} = O(1)$ and $\alpha \geq 0$ from refined similarity. Using (7.45) with $K = K_{sub}$ and $\beta = \beta_{sub}$,

$$n(L) = \frac{\Pi_1}{K_{sub}}\,L^{-(11/3+\alpha)}. \tag{7.48}$$

Downloaded from https://www.cambridge.org/core. IP address: 2.34.25.197, on 04 May 2026 at 12:12:30, subject to the Cambridge Core terms of use, available at https://www.cambridge.org/core/terms. https://doi.org/10.1017/jfm.2026.11233

In the case with removal $q = 1/2$ (on average, one of the two daughters is removed), using (7.46) with $K = K_{sub}$ and $\beta = \beta_{sub}$,

$$n(L) = \frac{2\,\Pi_1^{\downarrow}}{K_{sub}\,\mathcal{L}}\,L^{-(8/3+\alpha)}. \tag{7.49}$$

7.10.2. *Scaling law in the supercritical bulk*

For L above the critical span, the hazard is eddy-time limited, $h(L) = \kappa_h/\tau_L(L)$ with $\tau_L(L) \sim \bar{\varepsilon}^{-1/3} L^{2/3}$, i.e.

$$h(L) = K_{sup}\,L^{\beta_{sup}}, \qquad \beta_{sup} = -\frac{2}{3}, \qquad K_{sup} = \kappa_h\,\bar{\varepsilon}^{1/3}, \tag{7.50}$$

where $\kappa_h = O(1)$. Equation (7.45) with $K = K_{sup}$ and $\beta = \beta_{sup}$ gives

$$n(L) = \frac{\Pi_1}{K_{sup}}\,L^{-4/3}, \qquad \max\{L_{min},\ \ell_c^{(1)}\} \ll L \ll \mathcal{L}. \tag{7.51}$$

In the case of removal $q = 1/2$, using (7.46) with $K = K_{sup}$ and $\beta = \beta_{sup}$,

$$n(L) = \frac{2\,\Pi_1^{\downarrow}}{K_{sup}\,\mathcal{L}}\,L^{-1/3}, \qquad \max\{L_{min},\ \ell_c^{(1)}\} \ll L \ll \mathcal{L}. \tag{7.52}$$

8. Scaling summary

In this section we collect the main scaling results established in the paper, both for the self-similar transient response and for the stationary bulk with sources/sinks. In what follows, the hazard is written $h(L) = K\,L^{\beta}$ with regime-dependent β.

8.1. *Kinematic response*

Here we report the results of the kinematic response at scale L: how the coarse-grained turbulent forcing bends a single element, quantified by the peak curvature $\kappa^\star(L)$ and by the curvature moments $M_p(L)$. These laws are determined solely by beam mechanics and turbulence statistics; they do not rely on the kinetic (population-balance) model. In plain words,

$$\kappa^\star(L) \sim \frac{\xi_\perp}{EI}\,\langle \varepsilon_L^{1/3}\rangle_b\,L^{7/3}, \qquad M_p(L) \sim \left(\frac{\xi_\perp}{EI}\right)^p L^{7p/3}\,\langle \varepsilon_L^{p/3}\rangle_b. \tag{8.1}$$

Under refined similarity,

$$\langle \varepsilon_L^{p/3}\rangle_b = \bar{\varepsilon}^{p/3}\left(\frac{L}{\mathcal{L}}\right)^{\tau(p/3)}, \qquad \alpha \equiv \tau(1/3), \tag{8.2}$$

we finally obtain

$$M_p(L) \sim \left(\frac{\xi_\perp}{EI}\right)^p \bar{\varepsilon}^{p/3}\,\mathcal{L}^{-\tau(p/3)}\,L^{7p/3+\tau(p/3)}, \tag{8.3}$$

or, in the dimensionless form,

$$\widehat{M}_p^{(3)}(L) \equiv \frac{M_p(L)}{M_3(L)^{\,p/3}} \sim \left(\frac{L}{\mathcal{L}}\right)^{\tau(p/3)}, \qquad p > 0. \tag{8.4}$$

Downloaded from https://www.cambridge.org/core. IP address: 2.34.25.197, on 04 May 2026 at 12:12:30, subject to the Cambridge Core terms of use, available at https://www.cambridge.org/core/terms. https://doi.org/10.1017/jfm.2026.11233

8.2. *Self-similar transient regime*

Let $x \equiv L/L_*(t)$ and $n(L, t) = L_*(t)^{-2} F(x)$ be the self-similar description in the deep-cascade regime $L_* \ll \mathcal{L}$. The fixed-shape function $F(x)$ exhibits branch-dependent asymptotics in the limits $x \to 0$ and $x \to \infty$.

8.2.1. *Small x*

$$\begin{cases} \text{subcritical } (\beta_{sub} = 5/3 + \alpha): & F(x) = F(0) + O(x^2), \quad F(0) > 0, \\ \text{supercritical } (\beta_{sup} = -2/3): & F(x) \sim C\, x^{\mu}, \quad \mu = m + \dfrac{2}{3} > 0 \ \text{ if } \rho(r) \sim c_m r^{m} \ (r \downarrow 0). \end{cases} \tag{8.5}$$

8.2.2. *Large x*

$$\begin{cases} \text{subcritical } (\beta_{sub} = 5/3 + \alpha): & F(x) \sim C_\infty\, x^{-2} \exp\Big(- \dfrac{x^{\beta_{sub}}}{\beta_{sub}\, c_{eff}} \Big), \\ \text{supercritical } (\beta_{sup} = -2/3): & F(x) \sim C_-\, x^{-2}\big(1 + O(x^{\beta_{sup}}) \ = C_-\, x^{-2}\big(1 + O(x^{-2/3}) \ . \end{cases} \tag{8.6}$$

8.2.3. *Branch-aware matching*

Since the hazard law switches at $L \simeq \ell_c$, the notion of 'large x' must be read within the active branch. Setting $x_c(t) \equiv \ell_c/L_*(t)$, the stretched-exponential tail with $\beta_{sub} = 5/3 + \alpha$ applies on $1 \ll x \ll x_c(t)$ and matches to the algebraic tail with $\beta_{sup} = -2/3$ for $x \gg x_c(t)$.

8.2.4. *Typical-size dynamics and time scales*

The geometric typical size obeys the lineage law

$$\frac{\mathrm{d}}{\mathrm{d}t} \ln L_*(t) = -\, c_{eff}\, h(L_*(t))\,, \qquad \int_{L_*(t)}^{L_*(0)} \frac{\mathrm{d}\ell}{\ell\, h(\ell)} = c_{eff}\, t. \tag{8.7}$$

Along the supercritical branch, $h(L) = \kappa_h\, \bar{\varepsilon}^{1/3} L^{-2/3}$, the start-up time from $\mathcal{L}$ to the critical span scales as

$$t(\mathcal{L} \to \ell_c) = \frac{3}{2\, c_{eff}\, \kappa_h}\, \bar{\varepsilon}^{-1/3} \Big(\mathcal{L}^{2/3} - \ell_c^{2/3} \Big)\,, \tag{8.8}$$

while in the subcritical branch, $h(L) = K_{sub}\, L^{\beta}$ with $\beta = 5/3 + \alpha > 0$, the halving time reads

$$t_{1/2}(L) = \frac{2^{\beta} - 1}{\beta\, c_{eff}\, K_{sub}}\, L^{-\beta}. \tag{8.9}$$

8.3. *Scaling laws in the stationary bulk*

No removal ($q = 1$). Constant length-moment flux $\varPi_1$ fixes the amplitude:

$$\varPi_1 = h(L)\, L^2\, n(L), \qquad n(L) = \frac{\varPi_1}{K}\, L^{-(\beta+2)}, \qquad \tau_1 = \beta + 2, \qquad L_{min} \ll L \ll \mathcal{L}. \tag{8.10}$$

Downloaded from https://www.cambridge.org/core. IP address: 2.34.25.197, on 04 May 2026 at 12:12:30, subject to the Cambridge Core terms of use, available at https://www.cambridge.org/core/terms. https://doi.org/10.1017/jfm.2026.11233

Using ℓ_c as regime splitter,

$$h_{sub}(L) = K_{sub}\, L^{5/3+\alpha}, \qquad \Rightarrow \qquad n_{sub}(L) \propto L^{-(11/3+\alpha)}, \tag{8.11}$$

$$h_{sup}(L) = K_{sup}\, L^{-2/3}, \qquad \Rightarrow \qquad n_{sup}(L) \propto L^{-4/3}. \tag{8.12}$$

With removal ($q = 1/2$). The in-layer flux just below $\mathcal{L}$ is $\Pi_1^{\downarrow} = \Pi_1/2$ and $\tau_{1/2} = \beta + 1$. Hence

$$n(L) = \frac{\Pi_1}{K\,\mathcal{L}}\, L^{-(\beta+1)}, \qquad L_{min} \ll L \ll \mathcal{L}, \tag{8.13}$$

and, with ℓ_c as splitter,

$$h_{sub}(L) = K_{sub}\, L^{5/3+\alpha}, \qquad \Rightarrow \qquad n_{sub}(L) \propto L^{-(8/3+\alpha)}, \tag{8.14}$$

$$h_{sup}(L) = K_{sup}\, L^{-2/3}, \qquad \Rightarrow \qquad n_{sup}(L) \propto L^{-1/3}. \tag{8.15}$$

9. Connection to observed scaling laws in environmental microfibres

Kooi *et al.* (2021) reported extensive datasets of environmental microfibres across aquatic compartments, consistently finding power-law size distributions in the range from tens of micrometres up to a few millimetres, with exponents between 2.1 and 3.3 and a mean slope $\simeq 2.68$. These empirical laws are robust but, as the authors note, lack a clear mechanistic explanation. In what follows we show how our turbulence-informed kinetic theory provides a quantitative interpretation of these observations by placing the system under controlled physical conditions.

We consider aged polyethylene terephthalate (PET) as the representative polymer, motivated by its widespread occurrence in textile-derived microfibres and its prominence among the polymers identified by Kooi *et al.* (2021) . The Young's modulus $E \simeq 3\,\text{GPa}$ and fracture strain $\varepsilon_{frac} \simeq 1$ (Panowicz *et al.* 2021), giving a fracture curvature $\kappa_{frac} = \varepsilon_{frac}/a$. The fibres are embedded in water with kinematic viscosity $\nu = 10^{-6}\,\text{m}^2\,\text{s}^{-1}$ and dynamic viscosity $\mu = 10^{-3}\,\text{Pa s}$, subject to energetic turbulence with mean dissipation rate $\bar{\varepsilon} = 10^{-3}\,\text{m}^2\,\text{s}^{-3}$, representative of surf-zone (Feddersen 2012) and breaking-wave conditions in coastal seas, which are widely recognised as primary environments for fibre fragmentation before subsequent transport and dispersal. The dependence on $\bar{\varepsilon}$ is comparatively weak, scaling only as $\bar{\varepsilon}^{-1/4}$ in (7.25), so this choice is not critical for the following estimates.

Two diameters are examined, $d = 10$ m and $d = 50$ m, corresponding to radii $a = 5$ m and $a = 25$ m, which fall within the lower and intermediate range of fibre diameters documented in the datasets of Kooi *et al.* (2021).

The flexural rigidity follows $EI = E\,(\pi a^4/4)$, while the transverse drag is $\xi_\perp \simeq 4\pi\mu/(\ln \quad + \delta_\perp)$ with $\quad = L/a$ evaluated at $L = \ell_c$ and $\delta_\perp = O(1)$. For $d = 10$ m one finds $EI \simeq 1.47 \quad 10^{-12}\,\text{N}\,\text{m}^2$ and $\kappa_{frac} \simeq 2.0 \quad 10^3\,\text{m}^{-1}$, giving a critical span $\ell_c \simeq 9 \quad 10^{-3}\,\text{m}$ (≈ 1 cm), i.e. comparable to but slightly above the upper end of the observed range reported by Kooi *et al.* (2021). For $d = 50$ m one obtains $EI \simeq 9.2 \quad 10^{-10}\,\text{N}\,\text{m}^2$ and $\kappa_{frac} \simeq 4.0 \quad 10^2\,\text{m}^{-1}$, yielding $\ell_c \simeq 7.7 \quad 10^{-2}\,\text{m}$ (several cm), well above the lengths present in those datasets. In both cases the Kolmogorov scale is $\eta = (\nu^3/\bar{\varepsilon})^{1/4} \simeq 1.8 \quad 10^{-4}\,\text{m}$, so that the ratios are $\ell_c/\eta \simeq 53$ for $d = 10$ m and $\ell_c/\eta \simeq 430$ for $d = 50$ m. Thus, the inertial-range separation $\eta \ll \ell_c$ is well satisfied for both diameters (up to $O(1)$ variations associated with the resistive-force theory (RFT) logarithm and orientation/orbit factors).

Downloaded from https://www.cambridge.org/core. IP address: 2.34.25.197, on 04 May 2026 at 12:12:30, subject to the Cambridge Core terms of use, available at https://www.cambridge.org/core/terms. https://doi.org/10.1017/jfm.2026.11233

The lineage law (7.14) then provides the travel time from ℓ_c to η along the subcritical branch. Since the intermittency correction α is small, setting $\alpha = 0$ one obtains

$$t(\ell_c \to \eta) = \frac{1}{\beta\, c_{eff}}\, \tau_L(\ell_c) \left(\frac{\ell_c}{\eta}\right)^{\beta}, \qquad \beta = 5/3, \qquad \tau_L(L) = \bar{\varepsilon}^{-1/3} L^{2/3}, \tag{9.1}$$

with $c_{eff} \simeq \ln 2$ and $\kappa_{sub} \simeq 1$. Inserting the critical spans gives, numerically, $t \simeq 4.3$ min for $d = 10\quad \mathrm{m}$ ($\ell_c \simeq 9 \quad 10^{-3}$ m) and $t \simeq 10.6$ h for $d = 50 \quad \mathrm{m}$ ($\ell_c \simeq 7.7 \quad 10^{-2}$ m). Thus, in energetic surf conditions the cascade from ℓ_c to η proceeds on observable time scales, but slows markedly for larger diameters; combining $\ell_c \propto a^{9/7}$ with (9.1) yields the strong diameter dependence $t \propto a^3$ (for fixed fluid parameters). These numerical values may vary by factors of 2–3 owing to $O(1)$ orientation and hydrodynamic prefactors absorbed in the slender-body drag coefficient.

Under the constant-flux/no-removal baseline ($q = 1$), (7.45) gives $n(L) \propto L^{-(\beta+2)}$, i.e. $n(L) \propto L^{-(11/3+\alpha)} \approx L^{-3.7}$ for $\beta = 5/3 + \alpha$ with $\alpha \simeq 0.05$ – much steeper than the observed 2.1–3.3 (mean 2.68) of Kooi *et al.* (2021). By contrast, with horizontal-convergence removal ($q = 1/2$) one has $\tau_{1/2} = \beta + 1$, hence $n(L) \propto L^{-8/3-\alpha} \approx L^{-2.7}$, in striking agreement with the data. This points to removal processes as an important control on environmental microfibre size distributions; residual variability can arise from differences in effective retention q and from fits sampling sizes near/above ℓ_c (which include flatter supercritical contributions).

Using a consistent perpendicular drag (slender-body/RFT) and PET properties ($d = 10\,\mu\mathrm{m}$, $I = \pi d^4/64$, E as in § 3), with $\bar{\varepsilon} = 10^{-3}\,\mathrm{m^2 s^{-3}}$ and $\xi_\perp \simeq 1.5 \quad 10^{-3}\,\mathrm{N\,s\,m^{-2}}$, we obtain $L_{QS} \approx 1.5$ cm and $\ell_c \approx 1 - 2$ cm, i.e. the two scales are of the same order. Moreover, moderate departures from the strict $\tau_{visc}/\tau_L \to 0$ limit at $L \sim \ell_c$ affect only $O(1)$ prefactors and do not alter the L-exponents or the branch structure presented in this section.

10. Conclusions and perspectives

We have presented a mechanistic framework that directly connects hydrodynamic loading on a fibre to its curvature, fracture and population dynamics in turbulence. In the quasi-static response to random spanwise-odd forcing, the breakage hazard $h(L)$ is expressed in terms of the length scale L and the turbulent dissipation rate $\bar{\varepsilon}$, with two complementary regimes: subcritical, when $L < \ell_c$, where $h(L) \sim L^{5/3+\alpha}$, and supercritical, when $L > \ell_c$, where $h(L) \sim \bar{\varepsilon}^{1/3} L^{-2/3}$. The critical length ℓ_c emerges from the coupling between material properties and turbulent excitation, with explicit dependence on the flexural rigidity EI and the fracture curvature κ_{frac}. Inserting this hazard into a conservative fragmentation kinetics leads to a stationary bulk spectrum $n(L) \propto L^{-8/3-\alpha} \approx L^{-2.7}$, an exponent that already captures the experimental distributions available to date and thus provides a firm quantitative benchmark for both laboratory and numerical studies.

These results are directly relevant to the problem of microplastic generation in aquatic environments. A significant fraction of plastic debris is fibrous in nature, originating from textiles or technical filaments. For such objects, breakage is governed predominantly by viscous bending rather than impact. The present formalism connects environmental parameters ($\bar{\varepsilon}$), material properties (EI, κ_{frac}) and turbulence intermittency (α) to the evolution of fibre size, clarifying how macro- and meso-scale plastic fibres are transferred, through successive breakup events, into the micro-scale. Fragmentation conserves fibre mass and, at fixed diameter, it does not increase the lateral surface area per unit mass but it redistributes the material into many shorter and more readily dispersed fragments, which

Downloaded from https://www.cambridge.org/core. IP address: 2.34.25.197, on 04 May 2026 at 12:12:30, subject to the Cambridge Core terms of use, available at https://www.cambridge.org/core/terms. https://doi.org/10.1017/jfm.2026.11233

may increase the effective exposure of polymer surfaces to the surrounding fluid (e.g. leaching, biofilm colonisation, sorption). At the same time, the resulting length classes can enter the ingestion window of planktonic organisms, with direct implications for bioavailability and trophic transfer.

The explicit link between $\bar{\varepsilon}$ and $h(L)$ also allows for operational use of the model in environmental contexts. Fields of turbulent dissipation obtained from wave-ocean models or regional reconstructions can be projected onto length space through ℓ_c and $h(L)$, producing maps of breakage intensity and characteristic downshift times $t^*(L) \sim h(L)^{-1}$. Two practical consequences follow. First, the predicted bulk slope $8/3+\alpha$ offers a diagnostic for interpreting observed spectra: systematic deviations may indicate additional mechanisms such as collisions, fatigue or photo-degradation, or departures from binary splitting. Second, the combination of measured spectra and estimates of α enables an inverse use of the model, constraining effective pairs (EI, κ_{frac}) and typical $\bar{\varepsilon}$, thereby reconstructing mechanical exposure histories and discriminating among different sources.

The framework also highlights a dynamical threshold. Once the fibre length drops below ℓ_c, the scaling $h(L) \sim L^{5/3+\alpha}$ implies that the hazard decreases with decreasing size, so that the cascade systematically slows down as fragmentation proceeds toward the micro-scale.

Environmental and material modifiers remain crucial. Biofouling and photo-oxidation gradually reduce EI and can alter κ_{frac}, with the net effect of lowering ℓ_c and increasing hazard at fixed $\bar{\varepsilon}$. Boundary-layer shear and intermittency α further modulate effective exponents in space and time. These dependencies offer levers for seasonal scenarios and comparisons across habitats, from river plumes to coastal shelves and pelagic mixed layers.

Although parsimonious, the model can be extended along several directions. Incorporating stochastic and fatigue-induced thresholds, non-binary kernels and collision-driven events will refine the description in dense environments. Coupling with advection, settling and biofouling growth will enable predictions not only of size spectra but also of vertical distribution and residence times. Finally, calibration with experiments, high-resolution DNS and coordinated field campaigns, where $\bar{\varepsilon}$, mechanical properties and spectra are measured simultaneously, is essential to fix prefactors and consolidate predictive use.

In perspective, the quantitative bridge between turbulence statistics, fracture kinetics and emergent spectra provides a predictive basis for integrating the generation of fibrous microplastics into regional transport models. Such integration promises more robust estimates of hotspots, residence times and bioavailability, and yields mechanistic indicators for targeted monitoring and mitigation strategies.

Acknowledgements. The author gratefully acknowledges the valuable discussions with S. Brizzolara, S. Olivieri and M.E. Rosti.

Declaration of Interests. The author reports no conflict of interest.

Appendix A. Notation and symbols

This appendix summarises the principal symbols used throughout the paper; symbols are not necessarily listed in the order of appearance in the text.

Downloaded from https://www.cambridge.org/core. IP address: 2.34.25.197, on 04 May 2026 at 12:12:30, subject to the Cambridge Core terms of use, available at https://www.cambridge.org/core/terms. https://doi.org/10.1017/jfm.2026.11233

Symbol	Meaning
Lengths and geometric variables	
L	Current fibre span / fragment length (main size variable).
	Largest/injection span (upper bound of admissible parent sizes).
L_{min}	Small-size cutoff used as a lower bound in the kinetic model.
$L_*(t)$	Typical (mean) fragment length, $L_*(t) \equiv m_1(t)/m_0(t)$.
L_{dau}	Daughter length in a breakup event (so that $r \equiv L_{dau}/L_p$).
L_{tgt}	Target length used to define start-up/downshift times $t(L \rightarrow L_{tgt})$.
x	Similarity variable, $x \equiv L/L_*(t)$.
$x_{max}(t)$	Maximum similarity coordinate, $x_{max}(t) \equiv \quad /L_*(t)$.
$x_c(t)$	Critical similarity coordinate, $x_c(t) \equiv \ell_c^{(1)}/L_*(t)$.
s	Arclength coordinate along the fibre, $s \in [-L/2, L/2]$.
a	Fibre (effective) radius.
d	Fibre diameter, $d = 2a$.
	Aspect ratio, $\quad \equiv L/a \gg 1$.
η	Kolmogorov length scale ($\eta \sim (\nu^3/\bar{\varepsilon})^{1/4}$).
ℓ	Generic sub-span scale within the fibre, $\ell \leq L$.
L_{QS}	Quasi-static upper bound from $\tau_{visc} \ll \tau_L$.
ℓ_c	Mean-field critical span from the curvature-threshold balance.
$\ell_c^{(1)}$	Intermittency-corrected critical span based on $\kappa^\star(L)$.
$\ell_c^{(p)}$	Moment-based critical span, defined by $M_p(\ell_c^{(p)}) = \kappa_{frac}^p$.
Fibre mechanics and curvature	
E	Young's modulus.
I	Second moment of area (about the neutral axis).
EI	Flexural rigidity.
$T(s, t)$	Internal-bending torque (bending moment) along the fibre.
$T_{max}(t)$	Maximum bending torque along the span at time t.
$\kappa(s, t)$	Centreline curvature.
κ_{frac}	Material curvature threshold for brittle failure.
ε_{frac}	Fracture strain (used to estimate $\kappa_{frac} \sim \varepsilon_{frac}/a$ when stated).
κ_ℓ	Curvature contribution associated with a sub-span scale ℓ.
$\kappa_{blk}^{(b)}$	Block-peak curvature (maximum over time within block b).
$M_p(L)$	pth block moment, $M_p(L) \equiv \langle (\kappa_{blk}^{(b)})^p \rangle_b$.
$\kappa^\star(L)$	Typical block-peak curvature, $\kappa^\star(L) \equiv M_1(L)$.
$\kappa_{MF}^\star(L)$	Mean-field estimate (no intermittency).
$\widehat{M}_p^{(3)}(L)$	Normalised curvature moment, $\widehat{M}_p^{(3)}(L) \equiv M_p(L)/M_3(L)^{p/3}$.
Flow, drag and kinematics	
$\boldsymbol{u}(\boldsymbol{x}, t)$	Fluid velocity field.
$\phi(s)$	Relative velocity entering resistive-force drag, $\phi(s) \equiv u(r(s), t) - \dot{r}(s, t)$.
$u_s(r_0, t)$	Fibre midpoint (solid) velocity used in the decomposition of the residual velocity.
$u_{slip}(t)$	Midpoint slip velocity, $u_{slip}(t) \equiv u(r_0, t) - u_s(r_0, t)$.
$\boldsymbol{r}(s, t)$	Fibre centreline position.
$\boldsymbol{r}_0$	Midpoint position, $\boldsymbol{r}_0 \equiv \boldsymbol{r}(0, t)$.
$\delta\boldsymbol{r}(s)$	Midpoint-centred displacement, $\delta\boldsymbol{r}(s) \equiv \boldsymbol{r}(s, t) - \boldsymbol{r}_0$.
$\dot{\boldsymbol{r}}(s, t)$	Fibre material-point velocity.
$\boldsymbol{t}(s, t)$	Unit tangent vector, $\boldsymbol{t} \equiv \partial_s \boldsymbol{r}$, $\lVert \boldsymbol{t} \rVert = 1$.
$\boldsymbol{t}_0$	Midpoint tangent, $\boldsymbol{t}_0 \equiv \boldsymbol{t}(0, t)$.
$\boldsymbol{P}(s, t)$	Projector onto the local normal plane, $\boldsymbol{P} \equiv \quad - \boldsymbol{t}\boldsymbol{t}$.
$\boldsymbol{P}_0$	Midpoint projector, $\boldsymbol{P}_0 \equiv \quad - \boldsymbol{t}_0\boldsymbol{t}_0$.
	Identity tensor (distinguished from the scalar second moment of area I).
$\boldsymbol{n}_0$	Fixed midpoint unit normal used to define the signed normal load.
$\boldsymbol{S}_0$	Symmetric part of $(\boldsymbol{\nabla u})_0$ (strain-rate tensor at $\boldsymbol{r}_0$).
$\boldsymbol{W}_0$	Antisymmetric part of $(\boldsymbol{\nabla u})_0$ (rigid-rotation tensor at $\boldsymbol{r}_0$).

Table 1. For caption see next page.

Downloaded from https://www.cambridge.org/core. IP address: 2.34.25.197, on 04 May 2026 at 12:12:30, subject to the Cambridge Core terms of use, available at https://www.cambridge.org/core/terms. https://doi.org/10.1017/jfm.2026.11233

Symbol	Meaning
$_{0}$	Rotation vector associated with $\boldsymbol{W}_0$.
$\boldsymbol{U}_\perp(s,t)$	Residual normal velocity (translation/rotation removed and projected).
$U_L(t)$	Operational transverse velocity increment (shear amplitude) across span L.
(t)	Orientation angle entering cos (t) in the signed load amplitude.
$C^{(b)}$	Blockwise orientation factor, $C^{(b)} \equiv \lvert\cos\ {}^{(b)}\rvert \in [0, 1]$.
$\boldsymbol{f}(s,t)$	Hydrodynamic traction per unit length on the fibre.
$\xi_\perp, \xi_\parallel$	Normal/parallel resistive-force drag coefficients.
$\delta_\perp, \delta_\parallel$	$O(1)$ constants in the slender-body logarithmic drag formula.
μ	Dynamic viscosity.
ν	Kinematic viscosity.
u_{rms}	Root-mean-square velocity at the integral scale.
Loads and time scales	
$q(s,t)$	Signed normal load per unit length in the Euler–Bernoulli equation.
$q_0(t)$	Amplitude of the leading-order odd load, $q_{LO}(s,t) = q_0(t)\, s/L$.
$\bar{\varepsilon}$	Mean turbulent kinetic-energy dissipation rate.
τ_L	Eddy turnover time at scale L, $\tau_L \sim \bar{\varepsilon}^{-1/3} L^{2/3}$.
τ_{visc}	Viscous bending-relaxation time, $\tau_{visc} \sim \xi_\perp L^4/(EI)$.
ΔT	Block duration, $\Delta T \equiv c\, \tau_L$.
$q_{LO}(s,t)$	Leading-order spanwise-odd load profile, $q_{LO}(s,t) = q_0(t)\, s/L$.
$u_{thr}(L)$	Dynamic velocity threshold for deterministic fracture, $u_{thr}(L) \equiv (EI/\xi_\perp)\, \kappa_{frac}\, L^{-2}$.
T_0	Integral-scale turnover time used to non-dimensionalise time (defined by $t' \equiv t/T_0$).
$t(L_1 \to L_2)$	Lineage-downshift time, $t(L_1 \to L_2) = (1/c_{eff}) \int_{L_2}^{L_1} (\mathrm{d}\ell/\ell\, h(\ell))$.
$t_{1/2}(L)$	Halving time of the typical size, $t_{1/2}(L) \equiv t(L \to L/2)$.
c	Order-one prefactor in the block duration $\Delta T = c\, \tau_L$.
Intermittency and scaling statistics	
ε_L	Coarse-grained dissipation at scale L.
$S_p(L)$	pth-order structure function of the transverse increment across separation L.
ζ_p	Structure-function exponent, $S_p(L) \sim L^{\zeta_p}$.
$\tau(q)$	Moment-scaling function, $\langle(\varepsilon_L/\bar{\varepsilon})^q\rangle \sim (L/\ \ )^{\tau(q)}$.
α	Intermittency correction, $\alpha \equiv \tau(1/3) = \zeta_1 - 1/3$.
$y_1(L)$	Dimensionless loading, $y_1(L) \equiv \kappa^\star(L)/\kappa_{frac}$.
$C_2(L)$	Moment ratio, $C_2(L) \equiv M_2(L)/M_1(L)^2$.
γ_p	Inertial-range scaling exponent for curvature moments, $\gamma_p \equiv (7/3)p + \tau(p/3)$.
$\theta(L)$	Threshold ratio, $\theta(L) \equiv \kappa_{frac}/\kappa^\star(L) = 1/y_1(L)$.
Fragmentation kinetics	
$n(L,t)$	Fragment-length number density.
$h(L)$	Hazard (breakup rate) for fragments of length L.
$p_{block}(L)$	Probability of breaking within one block of duration ΔT.
$B(L \mid L_p)$	Daughter-length kernel (density of daughters of length L from a parent L_p).
L_p	Parent length.
r	Daughter-to-parent ratio, $r \equiv L/L_p \in (0, 1)$.
$\rho(r)$	Probability density of r (exchange-symmetric: $\rho(r) = \rho(1-r)$).
$m_k(t)$	kth moment of $n(L,t)$, $m_k(t) \equiv \int_0 \ L^k n(L,t)\, \mathrm{d}L$.
(t)	Similarity amplitude in $n(L,t) = \ (t)F(x)$.
$F(x)$	Self-similar (fixed-shape) profile of the rescaled distribution.
c_{eff}	Mean logarithmic shrinkage, $c_{eff} \equiv \ \ [-\ln r]$.
$S(L,t)$	External source term.
$\mathcal{S}(t)$	Survival probability up to time t in the block model (so that $\mathcal{S}(t) = \exp[-h(L)t]$).
$p_{block}^{(\mathrm{lb})}(L)$	Paley–Zygmund lower bound on $p_{block}(L)$ (used in hazard bounds).
$K(L_p)$	Expected daughter multiplicity, $K(L_p) \equiv \int_0^{L_p} B(L\mid L_p)\, \mathrm{d}L$ (for binary breakup $K \equiv 2$).
$\beta_k(L)$	Moment gain factor, $\beta_k(L) \equiv (1/L^k) \int_0^L \ {}^k B(\ \mid L)\, \mathrm{d}\ $.

Table 1. For caption see next page.

Downloaded from https://www.cambridge.org/core. IP address: 2.34.25.197, on 04 May 2026 at 12:12:30, subject to the Cambridge Core terms of use, available at https://www.cambridge.org/core/terms. https://doi.org/10.1017/jfm.2026.11233

Symbol	Meaning
C_F	Shape factor of the fixed profile F, relating mean length to typical size: $m_1/m_0 = C_F L^*$.
K	Power-law hazard prefactor in $h(L) = K L^{\beta}$ (not to be confused with $K(L_p)$).
β	Power-law hazard exponent in $h(L) = K L^{\beta}$.
κ_h	Order-one prefactor in the eddy-time-limited (supercritical) hazard (e.g. $h(L) = \kappa_h\, \bar{\varepsilon}^{1/3} L^{-2/3}$).
κ_{sub}	Order-one prefactor in the subcritical hazard closure.
K_{sub}	Subcritical hazard prefactor in $h(L) = K_{sub} L^{\beta_{sub}}$.
β_{sub}	Subcritical hazard exponent (prototype: $\beta_{sub} = 5/3 + \alpha$).
K_{sup}	Supercritical hazard prefactor in $h(L) = K_{sup} L^{\beta_{sup}}$.
β_{sup}	Supercritical hazard exponent (prototype: $\beta_{sup} = -2/3$).
$Q(L)$	Sink/removal term (when included).
Steady cascade with retention/removal	
ξ	Logarithmic length coordinate, $\xi \equiv \ln L$.
$\Delta\xi$	Logarithmic bin width in ξ (used for flux estimates).
q	Retention fraction of daughters that remain in the system (note: distinct from $q(s, t)$).
Π_1	Injection rate of the conserved length moment, $\Pi_1 \equiv \int_0 \; L\, S(L, t)\, \mathrm{d}L$.
$\Lambda_1(q)$	Retention factor in the mean downscale crossing per breakup event.
$J_q(L)$	Downscale length flux across L per unit time and per unit ξ (with retention q).
$\Pi_1^{\downarrow}$	Top-of-cascade in-layer flux (used in the $q = 1/2$ steady solution).
τ	Steady bulk exponent in the no-removal baseline ($q = 1$), $n(L) \propto L^{-\tau}$.
$\tau_{1/2}$	Steady bulk exponent for $q = 1/2$ (one daughter removed on average), with $\tau_{1/2} = \beta + 1$ in the subcritical bulk.
τ_q	Exponent of the steady power-law distribution with retention, $n(L) \propto L^{-\tau_q}$.
Notation and operators	
$\langle\ \rangle$	Ensemble/time average.
$\langle\ \rangle_b$	Average over blocks of duration ΔT.
$\mathbb{P}(\ )$	Probability.
$[\ ]$	Expectation (specified by a subscript when conditioning on a random variable, e.g. $\ _C$).
$\simeq B$	Approximate equality (subleading terms neglected).
$o(1)$	Little-o term: $f = o(1)$ means $f \to 0$ as the asymptotic parameter tends to its limit.
$O(1)$	Order-one quantity (independent of the asymptotic parameter).

Table 1. Summary of symbols used. Bold symbols denote vectors/tensors; subscript 0 denotes midpoint quantities; superscript (b) denotes a block index; $\langle\ \rangle$ denotes averaging and $\langle\ \rangle_b$ averaging over blocks.

Appendix B. Moment balances by Tonelli s theorem and convexity

This appendix derives the moment balance (7.10) and the sign properties (7.11).

Start from the breakage equation (no sources/sinks):

$$\partial_t n(L, t) = -\,h(L)\, n(L, t) + \int_L \; h(L_p)\, n(L_p, t)\, B(L \mid L_p)\, \mathrm{d}L_p, \qquad 0 < L < \mathcal{L}. \tag{B1}$$

For $k \geq 0$ define

$$m_k(t) \;\equiv\; \int_0 \; L^k\, n(L, t)\, \mathrm{d}L. \tag{B2}$$

Multiplying (B1) by L^k and integrating over $L \in (0, \mathcal{L})$ gives

$$\dot{m}_k(t) = -\int_0 \; h(L)\, n(L, t)\, L^k\, \mathrm{d}L + \int_0 \int_L \; h(L_p)\, n(L_p, t)\, B(L \mid L_p)\, L^k\, \mathrm{d}L_p\, \mathrm{d}L. \tag{B3}$$

Downloaded from https://www.cambridge.org/core. IP address: 2.34.25.197, on 04 May 2026 at 12:12:30, subject to the Cambridge Core terms of use, available at https://www.cambridge.org/core/terms. https://doi.org/10.1017/jfm.2026.11233

Since the integrand in the double integral is non-negative, Tonelli's theorem swaps the order and yields

$$\dot{m}_k(t) = -\int_0 \; h(L)\, n(L,t)\, L^k \,\mathrm{d}L + \int_0 \; h(L_p)\, n(L_p,t)\, \varPhi_k(L_p)\,\mathrm{d}L_p, \tag{B4}$$

with

$$\varPhi_k(L_p) \equiv \int_0^{L_p} L^k\, B(L \mid L_p)\,\mathrm{d}L, \qquad \beta_k(L_p) \equiv \frac{\varPhi_k(L_p)}{L_p^k}. \tag{B5}$$

Thus

$$\dot{m}_k(t) = \int_0 \; h(L)\, n(L,t)\, [\beta_k(L) - 1]\; L^k\,\mathrm{d}L. \tag{B6}$$

10. *Self-similar binary kernel*

For (7.9),

$$B(L \mid L_p) = \frac{2}{L_p}\, \rho\left(\frac{L}{L_p}\right), \qquad r \equiv \frac{L}{L_p} \in (0,1), \qquad \int_0^1 \rho(r)\,\mathrm{d}r = 1, \tag{B7}$$

one finds

$$\beta_k(L_p) = 2\int_0^1 r^k \rho(r)\,\mathrm{d}r = 2\,\langle r^k\rangle_\rho. \tag{B8}$$

In particular,

$$\begin{aligned} &\text{fragment multiplicity:} \quad \beta_0 = \int_0^{L_p} B(L \mid L_p)\,\mathrm{d}L = 2, \\ &\qquad\qquad \Rightarrow \quad \dot{m}_0(t) = \int_0 \; h(L)\, n(L,t)\,\mathrm{d}L \;\geq\; 0, \end{aligned} \tag{B9}$$

$$\begin{aligned} &\text{length conservation:} \quad \int_0^{L_p} L\, B(L \mid L_p)\,\mathrm{d}L = L_p \iff \langle r\rangle_\rho = \frac{1}{2} \iff \beta_1 = 1, \\ &\qquad\qquad \Rightarrow \quad \dot{m}_1(t) = 0. \end{aligned} \tag{B10}$$

If ρ is exchange-symmetric ($\rho(r) = \rho(1-r)$), then $\langle r\rangle_\rho = 1/2$ holds automatically. Moreover, for $k > 1$, strict convexity implies $2\langle r^k\rangle_\rho < 1$ (non-degenerate binary splits), hence $\beta_k < 1$ and therefore

$$\dot{m}_k(t) \;<\; 0, \qquad k > 1. \tag{B11}$$

Appendix C. Typical-size dynamics and equivalence of definitions

This appendix supports the typical-size dynamics: it provides a short 'lineage' derivation of the drift law (7.13)–(7.14), and shows that in a self-similar regime the arithmetic mean length m_1/m_0 tracks the geometric typical size $L_*(t)$ up to a time-independent shape factor.

Lineage argument for the geometric typical size

Consider a tagged lineage $L(t)$, i.e. the length of a fragment followed along its successive breakups. Under the standard fragmentation (memoryless) assumption, break events occur

Downloaded from https://www.cambridge.org/core. IP address: 2.34.25.197, on 04 May 2026 at 12:12:30, subject to the Cambridge Core terms of use, available at https://www.cambridge.org/core/terms. https://doi.org/10.1017/jfm.2026.11233

with instantaneous rate (hazard) $h(L(t))$, and upon a break the tagged fragment length is multiplied by a random daughter ratio $r \in (0, 1)$. For the self-similar binary kernel (7.9), r has density $\rho(r)$ and is independent of the pre-break length.

Over a short time increment $\mathrm{d}t$, either no break occurs (probability $1 - h(L(t))\,\mathrm{d}t$), or one break occurs (probability $h(L(t))\,\mathrm{d}t$) and then $L \mapsto rL$. Therefore, to leading order in $\mathrm{d}t$,

$$[\ln L(t+\mathrm{d}t) - \ln L(t)] = \quad [h(L(t))\,\mathrm{d}t] \quad [\ln r] + o(\mathrm{d}t), \tag{C1}$$

where $\quad [\ ]$ denotes ensemble expectation (and we used independence of r). Dividing by $\mathrm{d}t$ and letting $\mathrm{d}t \to 0$ yields the exact drift identity

$$\frac{\mathrm{d}}{\mathrm{d}t} \quad [\ln L(t)] = \quad [h(L(t))] \quad [\ln r]. \tag{C2}$$

To close this at the level of a single ‘typical size’, we use the standard mean-lineage approximation $\quad [h(L(t))] \simeq h(L_*(t))$, where $L_*(t)$ is defined later. Since $\quad [\ln r] < 0$, it is convenient to introduce the positive constant

$$c_{eff} \equiv \quad [-\ln r] = \int_0^1 (-\ln r)\,\rho(r)\,\mathrm{d}r \; > \; 0, \tag{C3}$$

so that $\quad [\ln r] = -c_{eff}$.

Define the geometric typical size as

$$L_*(t) \; \equiv \; \exp\big(\quad [\ln L(t)] \; . \tag{C4}$$

Then the drift identity gives the lineage law

$$\frac{\mathrm{d}}{\mathrm{d}t} \ln L_*(t) = -\,c_{eff}\, h\big(L_*(t) \; , \qquad \int_{L_*(t)}^{L_*(0)} \frac{\mathrm{d}\ell}{\ell\, h(\ell)} = c_{eff}\, t, \tag{C5}$$

which is (7.13)–(7.14) in the main text (written here with the compact label (C5)).

As a reference case, if breakup were always exactly midspan, $r \equiv 1/2$ and hence

$$c_{eff} = \ln 2. \tag{C6}$$

10. *Equivalence with the arithmetic mean length in a self-similar regime*

Assume that, in the deep-cascade regime, the solution admits the self-similar form $n(L, t) = \quad (t)\, F(L/L_*(t))$ (with fixed profile F and typical size $L_*(t)$). Define the kth length moment of the distribution as $m_k(t) \equiv \int_0^\infty L^k\, n(L, t)\,\mathrm{d}L$ (or equivalently with the finite upper cutoff $L \le \mathcal{L}$; the argument is unchanged). Changing variables $L = L_* x$ gives

$$m_k(t) = \int_0^\infty L^k\, n(L, t)\,\mathrm{d}L = \quad (t)\, L_*^{k+1}(t) \int_0^\infty x^k F(x)\,\mathrm{d}x, \tag{C7}$$

so the arithmetic mean fragment length satisfies

$$\frac{m_1(t)}{m_0(t)} = C_F\, L_*(t), \qquad C_F \equiv \frac{\int_0^\infty x\, F(x)\,\mathrm{d}x}{\int_0^\infty F(x)\,\mathrm{d}x} > 0. \tag{C8}$$

Thus m_1/m_0 and the geometric typical size L_* differ only by the time-independent shape factor C_F and therefore obey the same time law (C5) (equivalently (7.13) in the main text).

Appendix D. Fixed-shape equation: derivation

This appendix derives the autonomous fixed-shape (7.15) from the population-balance (7.7) in the freely decaying case ($S = Q = 0$), under a homogeneous hazard $h(L) =$

Downloaded from https://www.cambridge.org/core. IP address: 2.34.25.197, on 04 May 2026 at 12:12:30, subject to the Cambridge Core terms of use, available at https://www.cambridge.org/core/terms. https://doi.org/10.1017/jfm.2026.11233

$K\,L^{\beta}$ and the binary self-similar kernel (7.9). In (7.7), at fixed size L, the contribution $-\,h(L)\,n(L,t)$ decreases the density because fragments of length L break at rate $h(L)$ and therefore leave the size class L (this is why it is referred to as a loss contribution). Conversely, the integral term increases $n(L,t)$ because it accounts for daughters of size L created when larger parents $L_p > L$ break: for a given parent L_p, the quantity $B(L \mid L_p)\,\mathrm{d}L$ is the expected number of daughters in $[L, L+\mathrm{d}L]$, and integrating over all $L_p \in [L, \mathcal{L}]$ gives the total gain into the class L.

Insert the similarity ansatz

$$n(L,t) = L_*^{-2}(t)\;F(x), \qquad x \equiv \frac{L}{L_*(t)}, \tag{D1}$$

into (7.7) with $S = Q = 0$ and $h(L) = K\,L^{\beta}$. At fixed L, $x = L/L_*(t)$ depends on time through $L_*(t)$, so

$$\partial_t n(L,t) = \partial_t\bigl(L_*^{-2} F(x) \;= L_*^{-2}\left[-\frac{\dot{L}_*}{L_*}\,\bigl(2F + x\,F'(x)\;\right]. \tag{D2}$$

The loss-by-breakage term in (7.7) becomes

$$-h(L)\,n(L,t) = -K\,L^{\beta}\,L_*^{-2}F(x) = -K\,L_*^{\beta}\,x^{\beta}\,L_*^{-2}F(x). \tag{D3}$$

For the gain term in (7.7) we use the binary kernel (7.9), $B(L \mid L_p) = (2/L_p)\rho(L/L_p)$, and change variables $L_p = L_*(t)\,y$ (so $\mathrm{d}L_p = L_*\,\mathrm{d}y$). Introducing $x_{max}(t) \equiv \mathcal{L}/L_*(t)$, one finds

$$\begin{aligned}\int_L h(L_p)\,n(L_p,t)\,B(L \mid L_p)\,\mathrm{d}L_p &= \int_L \bigl(K\,L_p^{\beta}\;\bigl(L_*^{-2}F(L_p/L_*)\;\frac{2}{L_p}\rho\left(\frac{L}{L_p}\right)\mathrm{d}L_p \\ &= K\,L_*^{\beta}\,L_*^{-2}\int_x^{x_{max}(t)} y^{\beta-1}F(y)\,2\,\rho\left(\frac{x}{y}\right)\mathrm{d}y.\end{aligned} \tag{D4}$$

Collecting the time derivative, the loss contribution $-h(L)n(L,t)$, and the gain integral in (7.7) yields

$$-\frac{\dot{L}_*}{L_*}\,\bigl(2F + x\,F' \;= K\,L_*^{\beta}\left[-x^{\beta}F(x) + \int_x^{x_{max}(t)} y^{\beta-1}F(y)\,2\,\rho\!\left(\frac{x}{y}\right)\mathrm{d}y\right]. \tag{D5}$$

On the homogeneous branch $h(L) = K\,L^{\beta}$, the typical-size law (7.13) reduces to

$$-\frac{\dot{L}_*}{L_*} = c_{eff}\,K\,L_*^{\beta}, \tag{D6}$$

so the explicit factor $K\,L_*^{\beta}$ cancels in (D5), leaving an autonomous equation for F.

Finally, in the deep-cascade regime $L_* \ll \mathcal{L}$ one has $x_{max}(t) = \mathcal{L}/L_*(t) \gg 1$. In this limit the similarity profile is supported on $x \ll x_{max}$, and the upper limit in the gain integral can be extended to ∞ (the contribution from $y > x_{max}$ is absent in the finite-support problem and becomes negligible asymptotically). This yields the fixed-shape equation stated in (7.15).

REFERENCES

ALLENDE, S., HENRY, C. & BEC, J. 2018 Stretching and buckling of small elastic fibers in turbulence. *Phys. Rev. Lett.* **121** (15), 154501.

ALLENDE, S., HENRY, C. & BEC, J. 2020 Dynamics and fragmentation of small inextensible fibres in turbulence. *Phil. Trans. R. Soc. Lond. A* **378** (2175), 20190398.

Downloaded from https://www.cambridge.org/core. IP address: 2.34.25.197, on 04 May 2026 at 12:12:30, subject to the Cambridge Core terms of use, available at https://www.cambridge.org/core/terms. https://doi.org/10.1017/jfm.2026.11233

ANDERSON, T.L. 2017 *Fracture Mechanics: Fundamentals and Applications*, 4th edn. CRC Press.

ANDRADY, A.L. 2011 Microplastics in the marine environment. *Mar. Pollut. Bull.* **62** (8), 1596–1605.

BABLER, M.U., *et al.* 2015 Numerical simulations of aggregate breakup in bounded and unbounded turbulent flows. *J. Fluid Mech.* **766**, 104–128.

BÄBLER, M.U., MORBIDELLI, M. & BAŁDYGA, J. 2008 Modelling the breakup of solid aggregates in turbulent flows. *J. Fluid Mech.* **612**, 261–289.

BANASIAK, J., LAMB, W. & LAURENÇOT, P. 2019 *Analytic Methods for Coagulation-Fragmentation Models*, vol. I. Chapman & Hall/CRC.

BATCHELOR, G.K. 1970 Slender-body theory for particles of arbitrary cross-section in Stokes flow. *J. Fluid Mech.* **44** (3), 419–440.

BERTOIN, J. 2006 *Random Fragmentation and Coagulation Processes, Cambridge Studies in Advanced Mathematics*, vol. 102. Cambridge University Press.

BOUCHERON, S., LUGOSI, G. & MASSART, P. 2013 *Concentration Inequalities: A Nonasymptotic Theory of Independence*. Oxford University Press.

BRIZZOLARA, S., ROSTI, M.E., OLIVIERI, S., BRANDT, L., HOLZNER, M. & MAZZINO, A. 2021 Fiber tracking velocimetry for two-point statistics of turbulence. *Phys. Rev. X* **11** (3), 031060.

BROUZET, C., GUINÉ, R., DALBE, M.-J., FAVIER, B., VANDENBERGHE, N., VILLERMAUX, E. & VERHILLE, G. 2021 Laboratory model for plastic fragmentation in the turbulent ocean. *Phys. Rev. Fluids* **6** (2), 024601.

CHIARINI, A., ROSTI, M.E. & MAZZINO, A. 2024 Dynamics and applications of finite-size fibre-like objects in turbulent flows. *Eur. J. Mech. B/Fluids* **108**, 104–118.

COX, R.G. 1970 The motion of long slender bodies in a viscous fluid Part 1. General theory. *J. Fluid Mech.* **44** (4), 791–810.

DOUMIC, M., ESCOBEDO, M. & TOURNUS, M. 2018 Estimating the division rate and kernel in the fragmentation equation. *Ann. Inst. Henri Poincaré C Anal. Non Linéaire* **35** (7), 1847–1884.

ESCOBEDO, M., MISCHLER, S. & RODRIGUEZ RICARD, M. 2005 On self-similarity and stationary problem for fragmentation and coagulation models. *Ann. Inst. Henri Poincaré C Anal. Non Linéaire* **22** (1), 99–125.

FEDDERSEN, F. 2012 Observations of the surf-zone turbulent dissipation rate. *J. Phys. Oceanogr.* **42** (3), 386–399.

FRISCH, U. 1995 *Turbulence: The Legacy of A. N. Kolmogorov*. Cambridge University Press.

GRAY, J. & HANCOCK, G.J. 1955 The propulsion of sea-urchin spermatozoa. *J. Expl Biol.* **32** (4), 802–814.

HULBURT, H.M. & KATZ, S. 1964 Some problems in particle technology: a statistical mechanical formulation. *Chem. Engng Sci.* **19** (8), 555–574.

KALOGERAKIS, N., KARKANORACHAKI, K., KALOGERAKIS, G.C., TRIANTAFYLLIDI, E.I., GOTSIS, A.D., PARTSINEVELOS, P. & FAVA, F. 2017 Microplastics generation: onset of fragmentation of polyethylene films in marine environment mesocosms. *Frontiers Mar. Sci.* **4**, 84.

KIM, S. & KARRILA, S.J. 1991 *Microhydrodynamics: Principles and Selected Applications*. Butterworth-Heinemann.

KOLMOGOROV, A.N. 1962 A refinement of previous hypotheses concerning the local structure of turbulence in a viscous incompressible fluid at high Reynolds number. *J. Fluid Mech.* **13** (1), 82–85.

KOOI, M., PRIMPKE, S., MINTENIG, S.M., LORENZ, C., GERDTS, G. & KOELMANS, A.A. 2021 Characterizing the multidimensionality of microplastics across environmental compartments. *Water Res.* **202**, 117429.

LEYVRAZ, F. 2003 Scaling theory and exactly solved models in the kinetics of irreversible aggregation. *Phys. Rep.* **383** (2–3), 95–212.

LIGHTHILL, J. 1976 Flagellar hydrodynamics. *SIAM Rev.* **18** (2), 161–230.

LIU, J., LIU, Q., AN, L., WANG, M., YANG, Q., ZHU, B., DING, J., YE, C. & XU, Y. 2022 Microfiber pollution in the earth system. *Rev. Environ. Contam. Toxicol.* **260**, 13.

MARCHIOLI, C., ROSTI, M.E. & VERHILLE, G. 2026 Flexible fibers in turbulence. *Annu. Rev. Fluid Mech.* **58**, 167–192.

MCGRADY, E.D. & ZIFF, R.M. 1987 'Shattering' transition in fragmentation. *Phys. Rev. Lett.* **58** (9), 892–895.

OLIVIERI, S., MAZZINO, A. & ROSTI, M.E. 2022 On the fully coupled dynamics of flexible fibres dispersed in modulated turbulence. *J. Fluid Mech.* **946**, A34.

PANOWICZ, R., KONARZEWSKI, M., DUREJKO, T., SZALA, M., ŁAZIŃSKA, M., CZERWIŃSKA, M. & PRASUŁA, P. 2021 Properties of polyethylene terephthalate (PET) after thermo-oxidative aging. *Materials* **14** (14), 3833.

PETERSON, R.E. 1974 *Stress Concentration Factors*, 2nd edn. Wiley.

POWERS, T.R. 2010 Dynamics of filaments and membranes in a viscous fluid. *Rev. Mod. Phys.* **82** (2), 1607–1631.

Downloaded from https://www.cambridge.org/core. IP address: 2.34.25.197, on 04 May 2026 at 12:12:30, subject to the Cambridge Core terms of use, available at https://www.cambridge.org/core/terms. https://doi.org/10.1017/jfm.2026.11233

PUMIR, A. & WILKINSON, M. 2011 Orientation statistics of small particles in turbulence. *New J. Phys.* **13** (9), 093030.

RAMKRISHNA, D. 2000 *Population Balances: Theory and Applications to Particulate Systems in Engineering*. Academic Press.

ROSTI, M.E., BANAEI, A.A., BRANDT, L. & MAZZINO, A. 2018 Flexible fiber reveals the two-point statistical properties of turbulence. *Phys. Rev. Lett.* **121** (4), 044501.

SUARIA, G., ACHTYPI, A., PEROLD, V., LEE, J.R., PIERUCCI, A., BORNMAN, T.G., ALIANI, S. & RYAN, P.G. 2020 Microfibers in oceanic surface waters: a global characterization. *Sci. Adv.* **6** (23), eaay8493.

TANG, S.L., ANTONIA, R.A. & DJENIDI, L. 2023 Dual scaling and the n-thirds law in grid turbulence. *J. Fluid Mech.* **975**, A32.

TANG, S.L., ANTONIA, R.A., DJENIDI, L., DANAILA, L. & ZHOU, Y. 2017 Finite Reynolds number effect on the scaling range behaviour of turbulent longitudinal velocity structure functions. *J. Fluid Mech.* **820**, 341–369.

TANG, S.L., ANTONIA, R.A., DJENIDI, L. & ZHOU, Y. 2020 Scaling of the turbulent energy dissipation correlation function. *J. Fluid Mech.* **891**, A26.

TENNEKES, H. & LUMLEY, J.L. 1972 *A First Course in Turbulence*. MIT Press.

TIMOSHENKO, S.P. & GOODIER, J.N. 1970 *Theory of Elasticity*, 3rd edn. McGraw–Hill.

VANDENBERGHE, N. & VILLERMAUX, E. 2013 Geometry and fragmentation of soft brittle impacted bodies. *Soft Matt.* **9** (34), 8162–8176.

VELA-MARTÍN, A. & AVILA, M. 2022 Memoryless drop breakup in turbulence. *Sci. Adv.* **8** (50), eabp9561.

VILLERMAUX, E. 2007 Fragmentation. *Annu. Rev. Fluid Mech.* **39** (1), 419–446.

VILLERMAUX, E. 2025 Fragmentation: principles versus mechanisms. *Phys. Rev. Lett.* **135** (22), 228201.

VOTH, G.A. & SOLDATI, A. 2017 Anisotropic particles in turbulence. *Annu. Rev. Fluid Mech.* **49** (1), 249–276.

WEIBULL, W. 1951 A statistical distribution function of wide applicability. *J. Appl. Mech.* **18** (3), 293–297.

ZHAO, S., *et al.* 2025 The distribution of subsurface microplastics in the ocean. *Nature* **641** (8061), 51–61.

ZIFF, R.M. & MCGRADY, E.D. 1985 The kinetics of cluster fragmentation and depolymerisation. *J. Phys. A: Math. Gen.* **18** (15), 3027–3037.